



OPEN ACCESS

EDITED BY

Vanda Brotas,
University of Lisbon, Portugal

REVIEWED BY

Stella Psarra,
Hellenic Centre for Marine Research
(HCMR), Greece
Presentación Carrillo,
University of Granada, Spain

*CORRESPONDENCE

Pablo Serret

✉ pserret@uvigo.es

RECEIVED 15 May 2023

ACCEPTED 13 October 2023

PUBLISHED 30 October 2023

CITATION

Serret P, Lozano J, Harris CB, Lange PK, Tarran GA, Tilstone GH, Woodward EMS and Zubkov MV (2023) Respiration, phytoplankton size and the metabolic balance in the Atlantic gyres. *Front. Mar. Sci.* 10:1222895. doi: 10.3389/fmars.2023.1222895

COPYRIGHT

© 2023 Serret, Lozano, Harris, Lange, Tarran, Tilstone, Woodward and Zubkov. This is an open-access article distributed under the terms of the [Creative Commons Attribution License \(CC BY\)](https://creativecommons.org/licenses/by/4.0/). The use, distribution or reproduction in other forums is permitted, provided the original author(s) and the copyright owner(s) are credited and that the original publication in this journal is cited, in accordance with accepted academic practice. No use, distribution or reproduction is permitted which does not comply with these terms.

Respiration, phytoplankton size and the metabolic balance in the Atlantic gyres

Pablo Serret^{1*}, Jose Lozano¹, Carolyn B. Harris², Priscila K. Lange³, Glen A. Tarran², Gavin H. Tilstone², E. Malcolm S. Woodward² and Mikhail V. Zubkov⁴

¹Centro de Investigación Mariña da Universidade de Vigo, Departamento de Ecoloxía e Bioloxía Animal, Vigo, Spain, ²Plymouth Marine Laboratory, Plymouth, United Kingdom, ³Universidade Federal do Rio de Janeiro, Rio de Janeiro, Brazil, ⁴Scottish Association for Marine Science, Oban, United Kingdom

The balance between plankton photosynthesis (GPP) and community respiration (CR) in the euphotic zone (net community production, NCP) is an essential driver of the biological carbon pump. Deficient datasets and a lack of knowledge of the mechanisms regulating CR cause poor empirical models and oversimplified parameterisations that maintain NCP as one of the most important unknowns for projections of the carbon pump. One important unresolved issue is the unexpected lack of empirical relationships between CR and the biomass or size-structure of the phytoplankton, which undermines the use of remotely sensed observations to predict net community metabolism. Here we analyse the spatial variation of plankton metabolism, chlorophyll a concentration (Chla), pico- and nanophytoplankton abundance and size-fractionated primary production (¹⁴CPP) along a latitudinal (49°N–46°S) transect of 73 stations across the Atlantic Ocean (AMT-22 cruise). The use of depth-weighted rates (rates integrated to the depth of 0.1% PAR, divided by the regionally varying depth of integration) markedly improved the depiction of latitudinal patterns and the significance of relationships, over volumetric or integrated rates. Depth-weighted CR showed clear and consistent latitudinal patterns with relevance for the distribution of NCP. Depth-weighted Chla and CR exhibited a significant relationship ($CR_z = 1.42Chla_z - 0.21$, $r^2 = 0.69$, $N=37$, $p < 0.001$) with potential for the difficult prediction of CR. A general ratio of 1.42 $mmolO_2 mgChla^{-1} d^{-1}$ and a threshold Chla for net heterotrophy of ca. 0.25 $mgChla m^{-3}$ can be tentatively proposed for the Atlantic, although further analyses of spatial and seasonal variation are necessary. We observed unusually positive NCP rates in the central part of the N gyre, due to a marked decrease of CR in a patch of high *Synechococcus* spp. abundance and high ¹⁴CPP by large phytoplankton. However, no relationship was observed between size-fractionated ¹⁴CPP and CR or the GPP : CR ratio during the cruise, contradicting the hypothesis that food web functioning is determined by the phytoplankton size structure. Such independence, together with the persistence of distinct GPP : CR and ¹⁴CPP : NCP relationships in distinct biogeographic provinces suggest a resilience of trophic dynamics and the existence of alternative ecosystem states, whose implications for projections of the metabolic state of the ocean are discussed.

KEYWORDS

plankton, respiration, photosynthesis, net community production, phytoplankton size structure, ecosystem state, prediction

1 Introduction

Marine organisms play a key role in CO₂ storage in the ocean, mainly through the biological carbon pump (BCP), where the sinking of organic carbon produced in the illuminated upper ocean leaves a deficit of dissolved CO₂ near the surface that is compensated by air-sea diffusion of atmospheric CO₂ (e.g., Boyd et al., 2019). The BCP accounts for around 90% of the vertical dissolved inorganic carbon gradient in the ocean and in its absence, the atmospheric CO₂ concentration would be double its current value (Boyd et al., 2019). There is consensus that the BCP will change due to the alteration of nutrient fluxes and the combined effects of three interconnected drivers of change in the ocean: warming, deoxygenation and acidification. However, the magnitude and even direction of these changes are highly uncertain, partly due to knowledge gaps in the representation of the biological contribution to the BCP (Bindoff et al., 2019; Wilson et al., 2022).

The primary driver for the BCP is the accumulation of organic carbon in the surface ocean, whose magnitude and efficiency are determined by two key biological processes: photosynthesis and respiration. Photosynthesis by the phytoplankton is responsible of virtually all the production of organic matter in the ocean. However, not all the organic carbon photosynthesised in the euphotic layer (gross primary production: GPP) sinks to depth. The maintenance, growth and activity of the phytoplankton and of the heterotrophs that directly or indirectly feed upon them require metabolic energy that is mostly supplied through respiration, thus reducing the net amount of organic matter available. By determining the rate at which the sinking organic matter is lost, the respiration of the entire plankton community (CR, the aggregated respiration of the phytoplankton and heterotrophic organisms) regulates the efficiency of the BCP. The balance of these processes in the euphotic layer is net community production (NCP=GPP-CR), which represents the potential BCP, i.e. the net amount of GPP in the euphotic zone that is ultimately available for sinking to the deep ocean or for transfer through food webs. Despite its importance, the magnitude and variation of NCP over regional scales remains poorly resolved, especially in the oligotrophic open ocean (e.g., Ducklow and Doney, 2013), which is particularly important due to its current extent (~ 56% of the ocean's surface) and projected climate change-related increases in area and oligotrophication (Signorini et al., 2015, and references therein).

Accurate projections of NCP would require validated empirical models or robust parameterisations of CR or NCP, based on knowledge of their controlling mechanisms. None of these is available. GPP : CR relationships used to extrapolate and predict the metabolic state of the epipelagic ocean (e.g., del Giorgio et al., 1997; Duarte and Agusti, 1998; Williams, 1998; Serret et al., 2009; Westberry et al., 2012; Regaudie-de-Gioux and Duarte, 2013; Tilstone et al., 2015; Ford et al., 2021) produced conflicting results that maintained a heated debate of >15 years about the metabolic state (auto- vs. heterotrophic) of the oligotrophic ocean (Ducklow and Doney, 2013). The analysis of data from ten Atlantic Meridional Transect (AMT) cruises subsequently revealed that the oligotrophic ocean is neither auto- nor heterotrophic, but

functionally diverse (Serret et al., 2015), however the different GPP : CR relationships observed in the North (heterotrophic) and South (autotrophic) Atlantic gyres have little predictive power.

Regarding parameterisation, in stark contrast to knowledge on controls and feedbacks on primary production (e.g., Falkowski et al., 1998), the biogeochemical processes controlling CR and NCP are largely undetermined. A recent review of field and experimental studies from 1991 to 2020 found only 36 publications with some empirical information about plankton respiration regulation (Wikner et al., 2023), where temperature, followed by primary production and DOC appear as unique controlling factors. Temperature dependence is the main, if not the only controlling factor of respiration in coupled climate-carbon cycle models in the oxygenated ocean (Wilson et al., 2022; Pasquier et al., 2023). Higher temperature undoubtedly increases the kinetics of respiration, as it does with any chemical reaction, including photosynthesis (Morel et al., 1996; Behrenfeld and Falkowski, 1997; Bouman et al., 2005; Smyth et al., 2005; Robinson et al., 2018). However, photosynthesis is rarely predicted from temperature alone because this physiological control is often intertwined in a complex matrix of interacting ecological constraints (e.g., nutrient availability, light, cell size, taxonomic composition, competition, predation) that covary with the environment (e.g., stratification, circulation, wind patterns, distance to the coast, etc.), thus reducing the relevance of the chemically-driven impact of temperature. Similarly, it is also very unlikely that real-world rates of CR in the ocean are controlled by temperature alone, although respiration is certainly expected to increase with higher temperature. The root of this oversimplified parameterisation of CR compared to PP is our poor empirical knowledge of the biogeochemical processes that interact with temperature to determine respiration rates *in situ*.

One important reason for this poor knowledge on empirical patterns and models of CR and NCP on the one hand, and on controlling processes of CR and NCP on the other hand, is the very poor database of measurements in the ocean (Robinson and Williams, 2005; Regaudie-de-Gioux and Duarte, 2013). Two main approaches exist to measure NCP in the ocean: methods based on *in situ* changes in budgets of chemical tracers in the water column, and methods based on *in vitro* changes in O₂ concentration after incubations of small seawater samples.

In situ methods are greatly improving the spatial and temporal coverage of NCP measurements, especially after the growing fleet of sensors mounted on autonomous platforms (e.g., Claustre et al., 2020). Target accuracy and precision of oxygen concentration determination from optodes (~1 μmol kg⁻¹ and 0.5 μmol kg⁻¹, respectively, Gruber et al., 2010; Bittig et al., 2018; Vikström et al., 2019), and observational bias and error (~ 3% and 6%, respectively, Johnson et al., 2017; Mignot et al., 2019) are large compared to typical NCP rates in the oligotrophic ocean (≤ 0.5 mmolO₂ m⁻³ d⁻¹, Serret et al., 2015). This implies that long and large integrations of O₂ budgets are needed. These integrative NCP estimates are very necessary indeed, but ineffective to represent the rapid dynamics and spatial heterogeneity of biogeochemical processes and interactions driving the functioning of plankton ecosystems, which undermines the potential for projection of the BCP, e.g. in response to different climate change scenarios. In this regard, *in situ*

budget-based NCP estimations in the euphotic zone are especially difficult. This zone, which is particularly relevant for projections of the BCP (see above), is operationally defined as the layer in the water column from the surface to the depth of the 1% of photosynthetically available light (PAR), not corresponding to any physical boundary related to the structure of the water column. This implies that the upper mixed layer may cross above and below the euphotic depth during the long periods necessary for budget calculations, causing difficulties to discern the long-term biological impact on O₂ inventories (Haskell et al., 2020). Altogether, the uncertainty in euphotic zone NCP estimations based on O₂ budgets in the upper ocean is very high (e.g. Hull et al., 2016; Hemming et al., 2022; see also Bittig et al., 2018).

Direct methods based on *in vitro* O₂ changes after 24 h incubations allow resolving scales better-suited to study the control of CR and NCP in the euphotic zone of the ocean. However, they are time-consuming and prone to manipulation biases due to lengthy sample handling protocols or potential “bottle effects” on the incubated communities. The ensuing paucity of *in vitro* data explains why large-scale and generalised patterns of plankton metabolism have been searched through meta-analyses of combined results from independent studies (e.g., Regaudie-de-Gioux and Duarte, 2013; Serret et al., 2015). Unbiased meta-analyses require datasets that are highly consistent in terms of accuracy and precision, which is a challenge for a method that combines a high potential for biases and a need for high precision to detect the minor changes in seawater O₂ concentration. For instance, measuring a rate of 0.4 mmolO₂ m⁻³ d⁻¹, typical of the oligotrophic open ocean, requires an interval of confidence ~0.3 mmolO₂ m⁻³ d⁻¹, especially for the critical determination of the positiveness or negativeness of NCP; this implies a coefficient of variation in the replicated measurements of oxygen concentration in the initial and incubated samples of ~0.05% (assuming a seawater concentration of 225 mmolO₂ m⁻³, 4 replicates and p=0.05). The most extensive collection of independent published and unpublished plankton metabolism data (Regaudie-de-Gioux and Duarte, 2013; <http://dx.doi.org/10.20350/digitalCSIC/220>) evidences that these requirements are not always met. Only 58% of the CR and NCP measurements reported (2116 out of 3634 CR data and 2226 out of 3849 NCP data) are presented with any indication of statistical dispersion. As the magnitude of the standard error (s.e.) of metabolic rates is difficult to assess, we have compared the s.e. relative to the magnitude of NCP in the 2226 data in the combined dataset of Regaudie-de-Gioux and Duarte (2013) with the 973 data points from 10 Atlantic Meridional Transect cruises (AMT11-18, AMT21-22), which resulted from the concerted effort of a small group of researchers following the same protocols (Serret et al., 2015). This comparison evidences striking differences in precision, with many data in the combined dataset whose s.e. are too large (Figure 1A), especially at low NCP values. Accuracy of NCP measurements is even more difficult to assess, because no standard exists for metabolic rates. However, absolute bounds can be derived from purely physiological constraints, based on the biomass and maximum photosynthetic efficiency of the phytoplankton. The maximum photosynthetic rate per unit chlorophyll-a (Chla) in the global ocean (~23 mmolO₂ mgChla-1

d-1, assuming 10 h of light and a PQ=1.1; Falkowski, 1981; Marra, 2012) and in oligotrophic ecosystems (~5 mmolO₂ mgChla-1 d-1, assuming 10 h of light and a PQ=1.1; Karl et al., 2002; Marra et al., 2007) set two such bounds for net primary production (NPP). As NCP is < NPP (NCP=NPP-heterotrophic R), NCP values considerably far from 5 mmolO₂ mgChla-1 d-1 are very unlikely in the gyres, and values near or above 23 are physiologically impossible. To minimise the impact of differences in phytoplankton biomass or light and nutrient fields on photosynthetic efficiency (Laws et al., 1987), we have compared the Chla : NCP ratios in the two subsets of data from the upper 10 m in unproductive ecosystems where Chla concentration was < 0.5 mg m⁻³ within the AMT latitude-longitude ranges (Figure 1B). While most AMT data are very close to, and below the 5 line, a large dispersion is observed along a similar Chla range in the independent observations gathered in Regaudie-de-Gioux and Duarte (2013), with some data that appear highly improbable, not to say physiologically impossible. These differences in precision and accuracy translate into noticeable differences in the representations of both the variability and latitudinal trend of NCP in the Atlantic Ocean (Figures 1C, D), and may partly explain the sustained disagreements and high uncertainty in regional estimations of NCP based on *in vitro* changes in O₂ concentration (Duarte et al., 2013; Williams et al., 2013).

A further shortcoming of meta-analyses is that small-scale patterns that are necessary to decipher the dynamic, often episodic and patchy co-variation of plankton metabolism with potential controlling factors, tend to be blurred in the grand averages or general trends (e.g. GPP : CR relationships). Our joined analysis of ten AMT datasets (8-37 stations per cruise) collected over >10 years (2000 to 2012) revealed consistent differences in GPP : CR relationship and metabolic state between the similarly oligotrophic North (heterotrophic) and South (autotrophic) Atlantic gyres (Serret et al., 2015). However, it provided very little insight into the regulation of NCP and CR in the ocean. Similarly, Robinson and Williams (2005) highlighted the unexpected lack of relationship between Chla and CR, despite both maintenance respiration and heterotrophic activity being expected to increase with autotrophic biomass. Such lack of relationship, which undermines the use of remotely sensed Chla observations to predict community metabolism, was confirmed by Regaudie-de-Gioux and Duarte (2013). Moreover, these authors also found a weak Chla : GPP relationship (R² = 0.29, n=1111) that contrasts with the key role played by phytoplankton biomass in models of primary production in the ocean (Westberry et al., 2023 and references therein). Conceptual and mechanistic models have often predicted that phytoplankton size determines the organisation and functioning of food webs, which should reflect on GPP : CR ratios and NCP (see Smith and Kemp, 2001 and references therein). However, the relationship between CR or NCP and the phytoplankton size-structure remains unresolved (Serret et al., 2001; Smith and Kemp, 2001; Arbones et al., 2008; Soria-Piriz et al., 2017; Wang et al., 2018; Juranek et al., 2020; Lozano et al., 2021). One specific objective of this paper is to overcome the limitations of meta-analysis, studying the relationship of CR and NCP with the abundance and structure of the phytoplankton

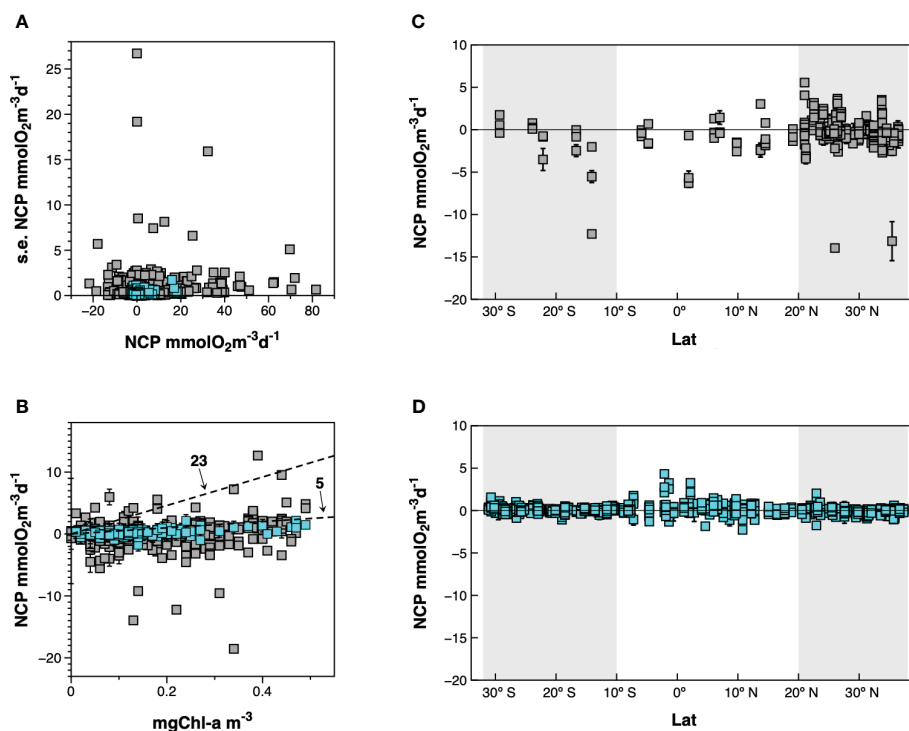


FIGURE 1

Comparison of precision and accuracy in two datasets in the Atlantic Ocean: grey squares, 25 published and unpublished records in the combined dataset of Regaudie-de-Gioux and Duarte (2013); blue squares, AMT11-22 data (Serret et al., 2015). (A) Comparison of standard errors relative to the magnitude of net community production. (B) Relationship between chlorophyll a concentration and net community production. Two physiological boundaries are identified based on the assimilation numbers that determine the maximum photosynthetic rate per unit chlorophyll a: ~23 mmol O₂ mg Chl-a d⁻¹ for the global ocean (Marra, 2012) and ~5 mmol O₂ mg Chl-a d⁻¹ characteristic of oligotrophic systems (Karl et al., 2002; Marra et al., 2007). NCP values considerably far from the 5 line are very unlikely in the gyres; values near or above the 23 line are physiologically impossible. (C) Latitudinal variation of net community production from the combined dataset in Regaudie-de-Gioux and Duarte (2013). (D) Latitudinal variation of NCP in Serret et al. (2015). The shadowed areas indicate the approximate location of the gyres. See text for details.

communities along a single latitudinal transect of the open Atlantic Ocean, with a focus on improved prediction.

We present here the detailed spatial variation of plankton metabolism along one selected Atlantic Meridional Transect (AMT) cruise, together with the variation of the physical and chemical environment and of the abundance and size-structure of the phytoplankton. We have selected the AMT22 cruise because, with 37 profiles of 5-6 depths down to the 0.1% PAR, including 12 stations in the Northern gyre and 9 in the Southern gyre, it is one of the most comprehensive datasets of plankton metabolism in the AMT series. Consistency of these data will be assessed by comparison with the entire AMT11-22 dataset (Serret et al., 2015) and also with a more coherent (in terms of precision and spatial coverage) subset of cruises (AMT11, 15, 21) to compare latitudinal patterns. AMT11, 15, 21 and 22 all took place during the boreal autumn; the very limited number of observations during boreal spring in the AMT11-22 dataset preclude an in-depth analysis of seasonality, however no evidence of a seasonal bias in regional patterns was observed (Serret et al., 2015). Our objectives are 1) to assess the validity of the conclusions, grand averages and general GPP : CR relationships derived from the meta-analysis of Serret et al. (2015) at ecological scales that are critical for prediction of changes in the metabolic state of the open ocean, 2) to improve the depiction of quasi-synoptic depth and latitudinal trends of GPP, CR

and NCP along the Atlantic Ocean, and 3) to study the relation between community metabolism and the phytoplankton abundance, community structure and ¹⁴C NPP; specifically, we will test the hypotheses that a) CR is poorly related to Chla (Robinson and Williams, 2005; Regaudie-de-Gioux and Duarte, 2013; Wikner et al., 2023, and references therein), b) CR is relatively invariant compared to GPP, meaning that the variation of NCP can be determined from GPP (Westberry et al., 2012; Duarte et al., 2013, and references therein), and c) the size-structure of phytoplankton communities determines food web functioning, reflecting on the GPP : CR ratio and NCP in the open ocean (Serret et al., 2001; Smith and Kemp, 2001 and references therein).

2 Methods

2.1 Sampling

A latitudinal (49°N–46°S) transect of 73 stations across the Atlantic Ocean (Atlantic Meridional Transect (AMT)-22 cruise) was conducted on RRS James Cook between Southampton, UK and Punta Arenas, Chile, between 10 October and 24 November 2012. Six biogeochemical provinces of the Atlantic Ocean were traversed: the mesotrophic North Atlantic Drift (NADR), Western Tropical

Atlantic (WTRA) and South Subtropical Convergence (SSTC), the oligotrophic South Atlantic Gyre (SATL), North Atlantic Tropical Gyre (NATR) and Northeast Atlantic Subtropical Gyre (NASTE) (Longhurst et al., 1995) (Figure 2). Each day, two stations were sampled at between 04:00 and 05:00 h, and between 13:00 and 14:00 h. Vertical profiles of temperature and conductivity were performed at every station using a stainless steel-framed Seabird CTD fitted to a rosette of 24x20 L Niskin bottles. The CTD system fluorometer was calibrated against extracted chlorophyll-a measurements from 250 mL seawater samples collected from the CTD Niskin bottles, following Welschmeyer (1994). Samples for nitrate concentration and abundance of pico- and nano-phytoplankton were collected at every station, while O₂ and ¹⁴C-derived metabolic rates were measured only during the early morning stations, which were spaced at approximately 350 km intervals. Vertical profiles of photosynthetic active irradiance (PAR, 400-700 nm) were calculated at the 13:00-14:00 h stations from casts of an optical profiler (SeaOPS).

2.2 Nitrate concentration

Micromolar nitrate concentrations were determined using a Technicon segmented flow colorimetric autoanalyser with methodology based on Brewer and Riley (1965) employing clean sampling and handling techniques. The 60ml HDPE sample bottles were 10% acid cleaned and then Milli-Q washed before the sample water was taken from the CTD bottles into these sample bottles, wearing vinyl, powder free gloves. The sample bottle was fitted

directly to the autosampler ready for analysis with no decanting of the samples to again stop any potential contamination. All samples were analysed within 90 min of sampling from the CTD-Rosette system.

2.3 Phytoplankton community structure and abundance by flow cytometry

Fresh seawater samples were collected in clean 250 mL polycarbonate bottles from the 20 L Niskin bottles from all CTD casts. Samples were stored in a refrigerator and analysed within 2 hours of collection. Fresh samples were measured using a Becton Dickinson FACSsort flow cytometer which characterised and enumerated *Prochlorococcus* sp. and *Synechococcus* sp. (cyanobacteria) and pico- and nano-eucaryote phytoplankton, based on their light scattering and autofluorescence properties (Tarran et al., 2006).

2.4 Gross primary production, net community production and community respiration

At the early morning stations, gross primary production (GPP), net community production (NCP) and community respiration (CR) were determined at six depths from *in vitro* changes in dissolved O₂ after 24 h light and dark bottle incubations. Sampling and incubation were carried out at the same depths,

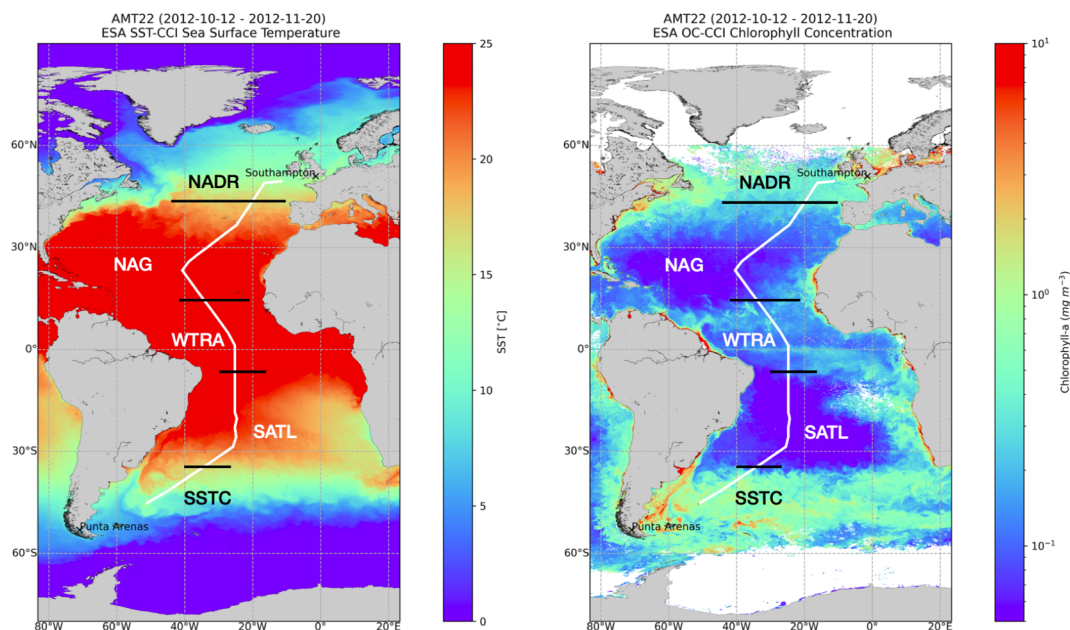


FIGURE 2

Track of Atlantic Meridional Transect 22 (AMT22) cruise, September–October 2012, overlaid on plots showing ESA Climate Change Initiative (CCI) Ocean Colour and Sea Surface Temperature data. The boundaries of biogeochemical provinces traversed (Longhurst, 1998) is shown. Each plot represents the median value for each pixel over the duration of the cruise. Earth observation data produced by the ESA Sea Surface Temperature Climate Change Initiative (SST-CCI) ESA Ocean Colour Climate Change Initiative (OC-CCI), courtesy of the NERC Earth Observation Data Acquisition and Analysis Service, the Ocean Biology Processing Group, NASA and European Space Agency.

simultaneously and under the same conditions as for ^{14}C incorporation experiments. Twelve 120 mL, gravimetrically calibrated, borosilicate glass bottles were carefully filled from each Niskin bottle using silicon tubing, overflowing by >250 mL. From each depth, four replicate 'zero-time' bottles were fixed immediately with Winkler reagents (1 mL of 3 M MnSO_4 and 1 mL of (8 M KOH + 4 M KI) solutions) added separately with an automatic multipipette. Two further sets of four replicates were incubated for 24 h in deck incubators. The incubators were maintained at surface temperature by pumping sea water from a depth of ~7 m through the upper light level incubators (97, 55, 33, 14, 7 & 3%) and from a chiller maintained at $\pm 1^\circ\text{C}$ of *in situ* temperature for the lower light level incubators (1 & 0.1%). One set of replicates was incubated in the dark, the other set in the equivalent irradiance to that found at the *in situ* sampling depth using various combinations of neutral density and blue plastic filters. Incubations always started at dawn and lasted 24 h. After the incubation period, the dark and light bottles were fixed with Winkler reagents. Dissolved O_2 concentration was determined with an automated Winkler titration system using potentiometric (Metrohm 716 DMS Titrimo) end-point detection (Oudot et al., 1988). Aliquots of fixed samples were delivered with a gravimetrically calibrated ~50 mL overflow ("Knudsen") pipette. Fixing, storage and standardization procedures followed the recommendations by Grasso et al. (1983). Production and respiration rates were calculated from the difference between the means of the replicate light and dark incubated bottles and zero-time analyses: $\text{NCP} = \Delta\text{O}_2$ in light bottles (mean of $[\text{O}_2]$ in 24 h light - mean zero time $[\text{O}_2]$); $\text{CR} = \Delta\text{O}_2$ in dark bottles (mean zero time $[\text{O}_2]$ - mean $[\text{O}_2]$ in 24 h dark); $\text{GPP} = \text{NCP} + \text{CR}$. The average standard error about the mean of both the NCP and CR rate measurements (which includes both experimental and biological variability) was 0.15 (n=214) $\text{mmolO}_2 \text{ m}^{-3} \text{ d}^{-1}$. Integrated values were obtained by trapezoidal integration of the volumetric data down to the depth of 0.1% surface incident photosynthetically active irradiance, excluding volumetric data whose standard error was more than twice the magnitude of the rate. The standard error of integrated GPP, CR and NCP was calculated through propagation of the random error in the volumetric measurements.

2.5 ^{14}C primary production

Water samples were taken from pre-dawn CTD deployments from 6 depths in the euphotic zone following the methods described in Tilstone et al. (2009). The samples were transferred from Niskin bottles to black carboys and sub-sampled into three 75 mL clear polycarbonate bottles and three black polycarbonate bottles; all bottles were pre-cleaned following JGOFS protocols (IOC, 1994), to reduce trace metal contamination. Each sample was inoculated with between 185 and 740 kBq (5 - 15 μCi) $\text{NaH}^{14}\text{CO}_3$ according to the biomass of phytoplankton, which was checked using the Chla profiles from the CTD cast. The polycarbonate bottles were transferred to the same on-deck (simulated *in situ*) incubation system used for NCP and CR incubations, using neutral density and blue filters to simulate subsurface irradiance over depth to 97%,

55%, 33%, 20%, 14%, 7%, 3%, 1% or 0.1% of the surface value and incubated from local dawn to dusk (10 - 16 h). To terminate the incubations, suspended material was filtered sequentially through 0.2 μm , 2 μm and 10 μm polycarbonate filters to measure pico-, nano- and microphytoplankton production respectively. A low vacuum pressure (20 cm Hg) was used to filter the samples to ensure that there was no loss of cells from the micro- or nano- to the pico- size fractions. The filters were exposed to concentrated hydrochloric acid fumes for 8-12 h, immersed in scintillation cocktail and ^{14}C disintegration time per minute (DPM) measured on board using a Packard, Tricarb 2900 liquid scintillation counter, with external standard and the channel ratio methods applied to correct for quenching.

3 Results

3.1 Thermal structure, nitrate and chlorophyll a concentrations

Figure 3 shows the latitudinal and vertical distributions of seawater temperature, nitrate and chlorophyll a concentration in the upper 250 m along the AMT22 cruise transect, which reflect the characteristics of the provinces traversed, identified here following Longhurst (1998). Although no single criterion can determine the exact location of regional nutriclines throughout such a varying scenario, the nitracline here is broadly defined as a gradient from 1 to 5 $\mu\text{mol NO}_3^- \text{ L}^{-1}$ through a vertical range of 25 m, although only the 1 $\mu\text{mol NO}_3^- \text{ L}^{-1}$ isoline (the uppermost part) is presented in figures.

The transect began in the south-eastern region of the NADR, where salinity and temperature were relatively low and homogeneous and nitrate was high through the water column. In the southern part of the NADR (47-43° N), a relatively weak thermocline was observed at the bottom of a shallow (~50 m depth) nitrate-depleted surface mixed layer. A broad frontal zone marked the transition from the NADR to the North Atlantic Gyre (NAG), which includes the westerlies NAST-E province (43-30° N) and the trades NATR province (30°-15° N) (Longhurst et al., 1995). The southward deepening of the nitracline reflected the increased surface warming and stratification through the gyre. The depth of the nitracline ranged from 75-100 m at the periphery of the gyre to 150-225 m at the centre of the NATR, where nitrate concentration was <0.05 $\mu\text{mol L}^{-1}$ from the surface down to ca. 100 m depth, indicative of very strong oligotrophic conditions. At the southern end of the NAG, the tilting of isolines of temperature and nitrate indicated the transition to the WTRA (15° N to 5° S), where the quasi-permanent upwellings and the increased surface warming created the most intense vertical gradients in temperature and nitrate. The strongest upwelling and shallowest nitracline (50 m depth) was found at the northern part of the province (centred around 10° N), caused by the divergence between the N equatorial current and counter current. The upwelling created by the equatorial divergence at ca. 2° S was less intense, possibly due to the seasonal weakening of equatorial trade winds (Grotsky et al., 2008). The associated convergence created between the N equatorial

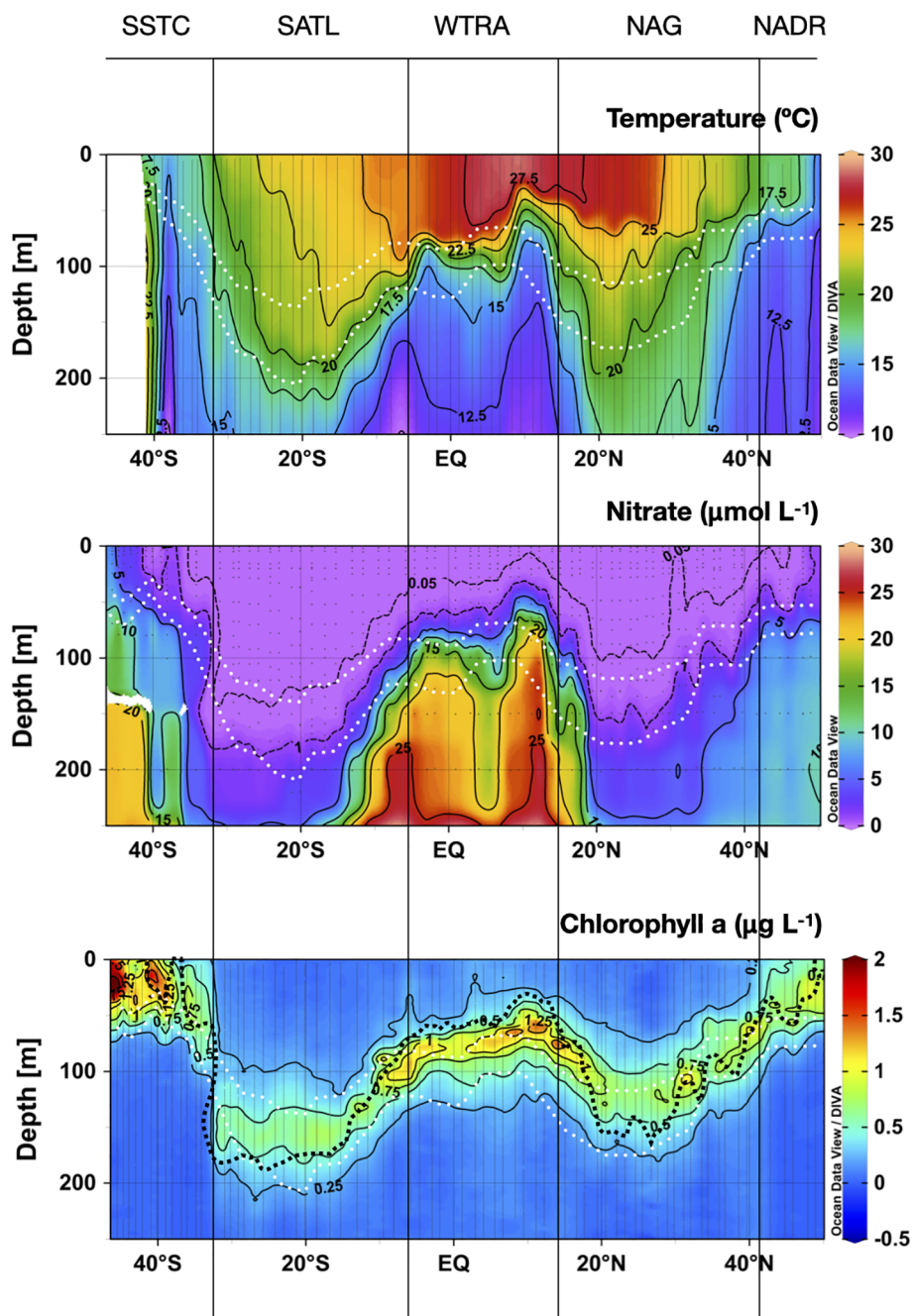


FIGURE 3
 Depth-latitude sections of temperature, nitrate concentration and chlorophyll a concentration during the AMT22 cruise. The white dotted lines are the depths of the 1 and 0.1%PAR. The black dotted line in the chlorophyll a contour plot is the depth of the nitracline. The approximate location of biogeographic provinces (Longhurst, 1998) is presented. Figures produced using Ocean Data View (Schlitzer, Reiner, Ocean Data View, <https://odv.awi.de>, 2022).

counter current and the S equatorial current can be identified in the sinking of surface seawater at ~5° N. South of the equatorial upwelling, the pycnocline progressively deepened and weakened as surface seawater became more saline (data not shown) and relatively colder. The transition to the SATL (5–32° S) was marked by such a progressive cooling and deepening of the surface mixed layer, with spatial patterns of thermohaline properties mirroring the NAG-WTRA transition. In the SATL, however, surface cooling was evident from the very northern

boundary. The fact that sampling was carried out during early boreal autumn in the NAG, and during early austral spring in the SATL (i.e., after long periods of surface warming and cooling, respectively) may contribute to these regional differences. The vertical gradients of temperature were weaker and more extended, and the mixed layer and nitracline reached deeper in the SATL than in the NAG. The thermocline and nitracline depths were maximum near the centre of the SATL at ~15–25° S. South of this area, a front marked the transition between the stratified waters of the SATL and

the colder and well-mixed waters of the SSTC (32–45°S). The reduced stratification and intense wind in this province caused a marked increase in nitrate concentration through the water column, with the $1 \mu\text{molNO}_3^- \text{L}^{-1}$ isoline reaching the surface.

Throughout the transect, the nitracline was always deeper relative to the light field in the gyres than in the productive provinces: it was above or near the depth of the 1% of photosynthetic available radiation (PAR) in the NADR, WATR and SSTC, but it was near the depth of the 0.1%PAR in the NAG and SATL. Such deep nutrient depletion reflects the intense oligotrophy in the gyres, and suggests relevant biological uptake of nitrate in these regions >50 m deeper than the 1%PAR.

Near-surface Chla maxima were only observed in the temperate NADR and SSTC, with almost three times higher concentration in the latter, possibly related to the higher stratification and lower nutrient concentration in the autumn NADR than in the spring SSTC. The deepening of the thermocline and nitracline into the N and S gyres was accompanied by a progressive deepening and weakening of the Chla maximum. Through both the NAG and SATL a deep Chla maximum (DCM) was observed extending 40–75 m above the nitracline. The maximum Chla concentration was lower in the SATL than in the NAG, and the absolute depth of the DCM, its vertical extent and upward distance from the nitracline were higher in the SATL than in the NAG. In the latter, the DCM was centred near the depth of the 1% PAR, as it was throughout most meso- and eutrophic environments, but the DCM in the SATL was found between the 1 and 0.1% PAR. This all indicates a higher degree of oligotrophy in the SATL, despite the fact that sampling was carried out during early boreal autumn in the NAG and during the austral spring in the SATL. Local increases in Chla concentration were observed at the DCM in the NAST-E section within the NAG (43–30° N) associated to local uplifts of the nitracline (e.g. at 32° N). Both surface and subsurface Chla concentrations increased approx. twice in the WTRA province, where the DCM followed the uplift of the thermo- and nitraclines by the regional upwelling. The shallowest DCM and highest Chla concentration were observed near the North equatorial divergence (around 10° N) where the most intense upwelling occurred.

3.2 Nano- and picoplankton abundance

Figure 4 shows the spatial distribution of the abundance of nano- and picoeukaryotic phytoplankton, *Synechococcus* spp. and *Prochlorococcus* spp. Abundance of nano- and picoeukaryotic cells was very high in the productive waters of the NADR, WTRA and SSTC, especially in the latter. In these provinces, the vertical distribution of cell abundance always matched the variation of Chla, with higher numbers in the surface layer of the high latitude provinces and in the DCM of the WTRA. Very low abundance of nano- and picoeukaryotic phytoplankton was observed in the two gyres, where higher numbers of picoeukaryotes were observed at the depths of the DCM; nanoeukaryotic phytoplankton was more abundant in the SATL than NAG and very low numbers were found in both gyres at the DCM.

The abundance of *Synechococcus* spp. was also very high in the Chla-rich surface NADR and SSTC, and in the upwelling system of the WTRA, but higher concentrations in the latter were observed above the DCM. Along the two gyres, the abundance of *Synechococcus* spp. was very low, especially at the DCM. An exception to these general patterns was observed in the central part of the NAG at around 23–28° N, where relatively high *Synechococcus* spp. numbers were observed in the upper 75 m.

The abundance of *Prochlorococcus* spp. was very low in high latitudes, especially in the highly productive SSTC, where it was practically absent. The highest abundances were found above the DCM in the WTRA, and relatively high numbers were observed in the upper part of the DCM within the two gyres (above the 1% PAR depth), where its distribution mirrored that of *Synechococcus* spp.

These observations agree with the general patterns in the Atlantic of higher abundance of *Synechococcus* spp. and eukaryotic phytoplankton in mesotrophic regions, and dominance of *Prochlorococcus* spp. in the gyres (Zubkov et al., 2000).

3.3 Plankton O₂ metabolism

3.3.1 Gross photosynthesis

3.3.1.1 Volumetric rates

GPP ranged from $0.01 \pm 0.12 \text{ mmolO}_2 \text{ m}^{-3} \text{ d}^{-1}$ at the bottom of the euphotic layer in the NAG to $9.83 \pm 0.34 \text{ mmolO}_2 \text{ m}^{-3} \text{ d}^{-1}$ near the surface at about 46° South (SSTC) (Figure 5). Throughout the transect, higher rates were always measured near the surface, with the highest values in the Chla-rich surface waters of the SSTC and NADR (>6 and >2 $\text{mmolO}_2 \text{ m}^{-3} \text{ d}^{-1}$, respectively), and relatively high rates above the DCM in the WTRA (>1.5 $\text{mmolO}_2 \text{ m}^{-3} \text{ d}^{-1}$).

GPP was also $\geq 1 \text{ mmolO}_2 \text{ m}^{-3} \text{ d}^{-1}$ near the surface in the transition zones at the periphery of the gyres, and decreased rapidly towards their centres, especially in the NAG. GPP at the DCM in the N and S gyres was very low, but measurable at most stations down to the depth of the 0.1%PAR (the average rates at the 0.1% PAR in the NAG and SATL were 0.18 ± 0.09 and $0.30 \pm 0.06 \text{ mmolO}_2 \text{ m}^{-3} \text{ d}^{-1}$, respectively; and the average standard error of measurements at that depth were 0.13 and 0.15 $\text{O}_2 \text{ m}^{-3} \text{ d}^{-1}$, respectively). In the NAG, GPP values $\leq 0.5 \text{ mmolO}_2 \text{ m}^{-3} \text{ d}^{-1}$ were measured between $\sim 32^\circ$ and 25° N through the euphotic layer, including the DCM. South of $\sim 26^\circ$ N, GPP rates $>0.5 \text{ mmolO}_2 \text{ m}^{-3} \text{ d}^{-1}$ were observed again in both the upper 50 m and at the DCM. Despite its lower Chla concentration and higher degree of oligotrophy, GPP was higher and less variable in the SATL than in the NAG, with rates typically $\geq 0.5 \text{ mmolO}_2 \text{ m}^{-3} \text{ d}^{-1}$ from the surface to the DCM. These values are in agreement with the average GPP rates at the NAG and SATL in the combined AMT11-22 dataset (Table 1).

3.3.1.2 Integrated rates

The average integrated GPP was highest in the SSTC ($196.6 \pm 7.3 \text{ mmolO}_2 \text{ m}^{-2} \text{ d}^{-1}$), followed by the WTRA, SATL, NAG and NADR provinces (114.0 ± 15.6 , 95.5 ± 26.2 , 58.3 ± 19.6 , $46.9 \pm 6.3 \text{ mmolO}_2 \text{ m}^{-2} \text{ d}^{-1}$ respectively) (Figure 6A). These results, where higher integrated GPP is observed in the oligotrophic SATL than in

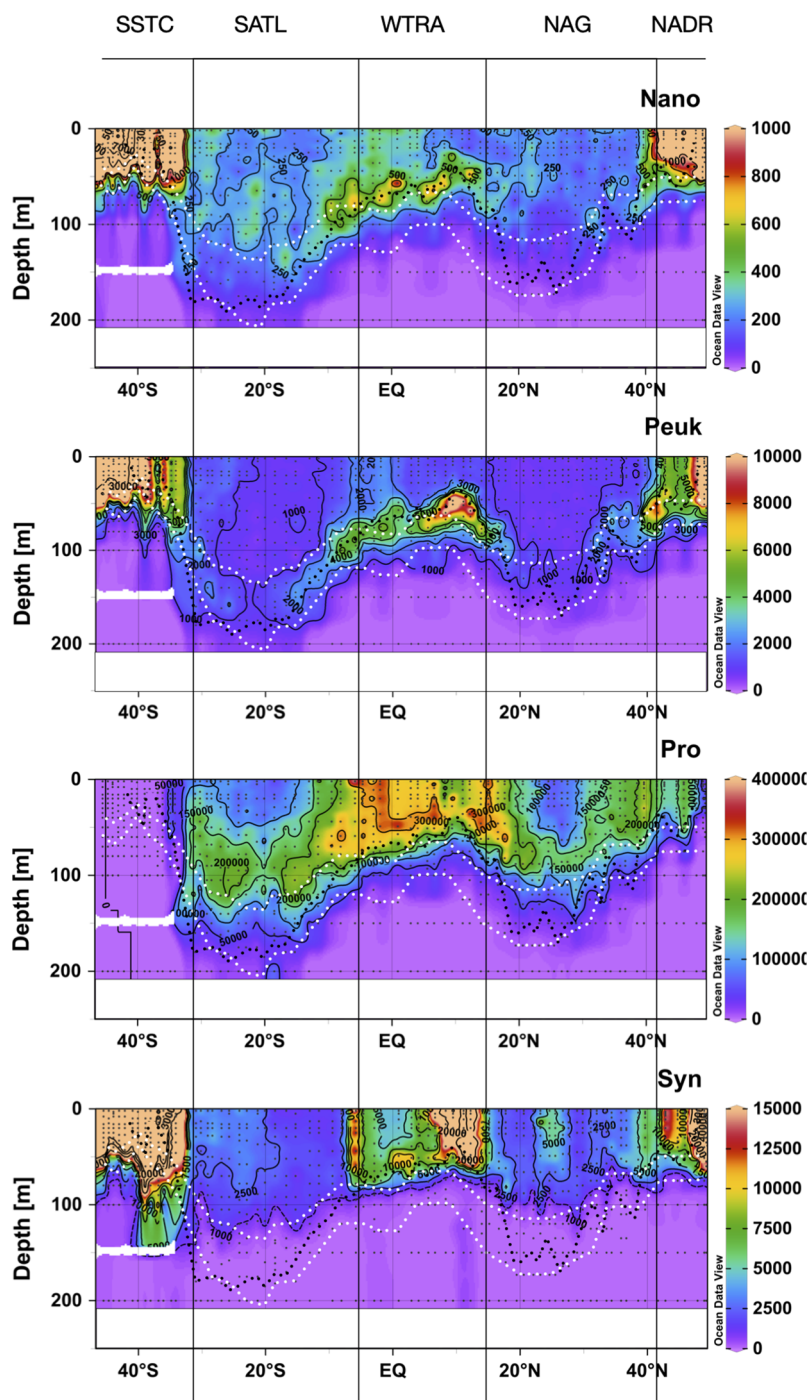


FIGURE 4

Depth-latitude sections of abundance (cells mL⁻¹) of nanoeukaryotic and picoeukaryotic phytoplankton, *Prochlorococcus* spp. and *Synechococcus* spp. during the AMT22 cruise. The white dotted lines are the depths of the 1 and 0.1%PAR. The black dotted line is the depth of the nitracline. The approximate location of biogeographic provinces (Longhurst, 1998) is presented. Figures produced using Ocean Data View (Schlitzer, Reiner, Ocean Data View, <https://odv.awi.de>, 2022).

the mesotrophic NADR, partly result from the regional differences in depth of integration, i.e., in the depth at which the incident light reached the 0.1% in each biogeographic province (see Figure 5). When integrated rates are divided by the depth of integration at the respective sampling stations, the spatial variation of the depth-weighted GPP (GPP_Z, which represents the average GPP rate across the euphotic layer) conforms well with the expectations based on

the general productivity of the provinces: the highest average GPP_Z was measured in the SSTC (2.78 ± 0.16 mmolO₂ m⁻³ d⁻¹), followed by the WTRA, NADR, SATL and NAG (1.20 ± 0.19 , 0.99 ± 0.15 , 0.63 ± 0.16 , 0.5 ± 0.16 mmol O₂ m⁻³ d⁻¹ respectively). Depth-weighting of integrated GPP also brings the magnitude and variation of AMT22 rates very close to those in previous AMT cruises (Figure 6B). For this comparative exercise we have selected

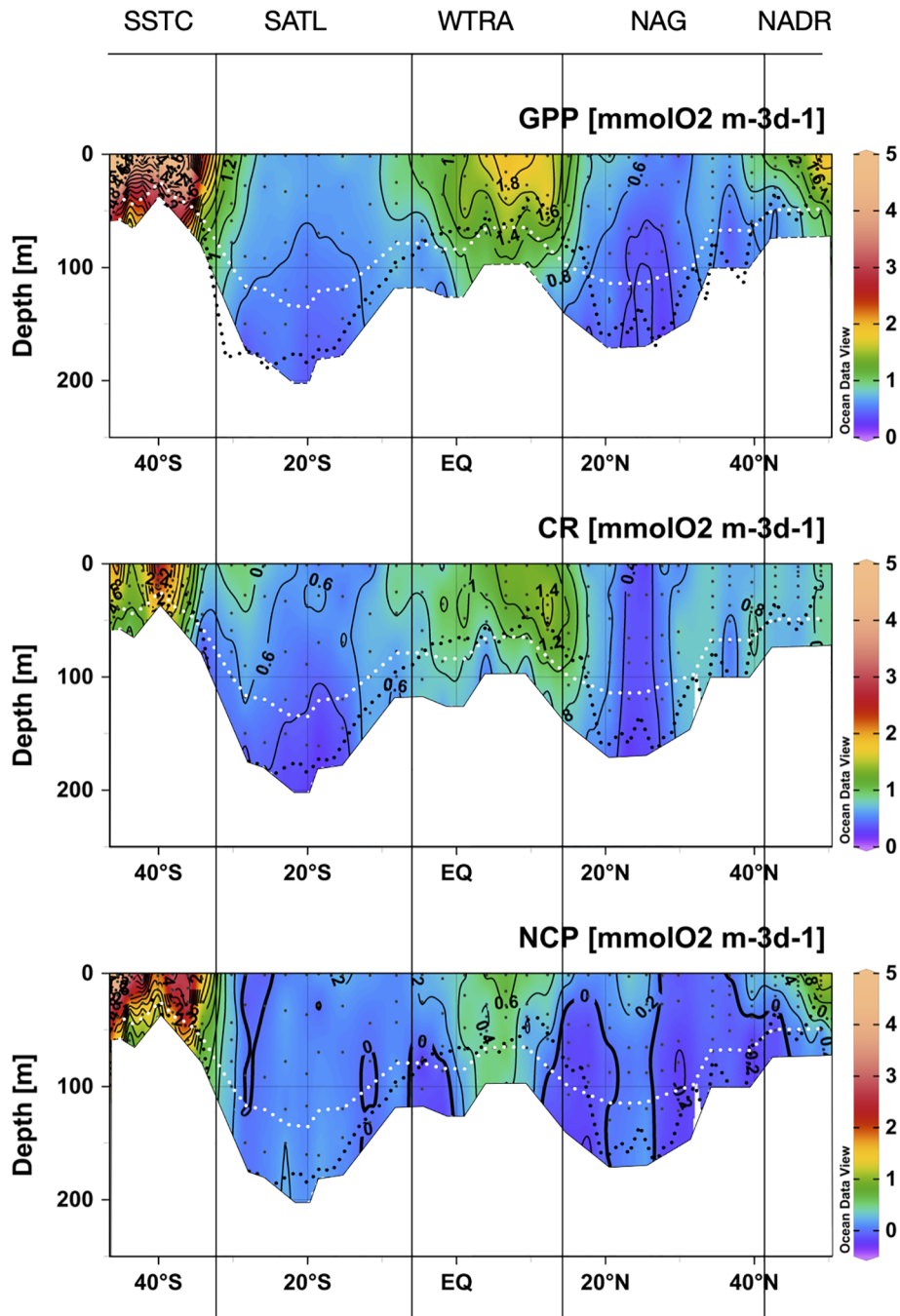


FIGURE 5

Depth-latitude sections of gross primary production, community respiration and net community production during the AMT22 cruise. The black dotted line is the depth of the nitracline. The white dotted line is the depth of the 1%PAR. The blanked area is the location of the deepest sample of each profile, at the depth of the 0.1%PAR. The approximate location of biogeographic provinces (Longhurst, 1998) is presented. Figures produced using Ocean Data View (Schlitzer, Reiner, Ocean Data View, <https://odv.awi.de>, 2022).

from the AMT11-22 dataset, those cruises with a continuous record of data through the regions studied here (AMT11-15-21), which ensures the consistency of zonal averages. GPP_z rates in the AMT22 and the AMT11-15-21 datasets depict very similar W-shaped latitudinal trends, in a much better agreement with the latitudinal variation of the nitracline than the variation of GPP_{int} , with more sensible differences between meso- and oligotrophic regions and lesser differences between the two gyres (Figures 6A, B). Moreover,

the relationship between depth-weighted Chla and GPP_z ($GPP_z = 4.53Chla_z - 0.59$; $r^2 = 0.88$; $n=37$) markedly improved over the poor volumetric (not shown) and integrated relationships (Figures 7A, B), confirming the value of representing biogeographic patterns with depth-weighted, rather than volumetric or integrated variables. The significant $Chla_z : GPP_z$ relationship shows little regional differences, despite the marked differences in euphotic, pycnocline, nitracline and DCM depths that

TABLE 1 Average (\pm s.e.) integrated ($\text{mmolO}_2 \text{ m}^{-2} \text{ d}^{-1}$) and depth-weighted ($\text{mmolO}_2 \text{ m}^{-3} \text{ d}^{-1}$) metabolic rates in the NAG and SATL in the combined AMT11-22 dataset (Serret et al., 2015) and in the AMT22 alone.

	NAG		SATL	
	Serret et al. (2015) autumn	AMT22	Serret et al. (2015) spring	AMT22
GPP_{int}	55.7 ± 3.2	71.17 ± 9.24	70.8 ± 2.6	116.1 ± 6.63
CR_{int}	72.0 ± 3.5	74.26 ± 10.49	58.4 ± 3.7	93.15 ± 2.69
NCP_{int}	-16.3 ± 2.5	-3.27 ± 5.77	12.3 ± 2.4	23.98 ± 6.93
GPP_Z	0.56 ± 0.02	0.56 ± 0.06	0.55 ± 0.02	0.69 ± 0.06
CR_Z	0.68 ± 0.03	0.59 ± 0.07	0.48 ± 0.02	0.55 ± 0.04
NCP_Z	-0.12 ± 0.02	-0.03 ± 0.04	0.06 ± 0.02	0.14 ± 0.04

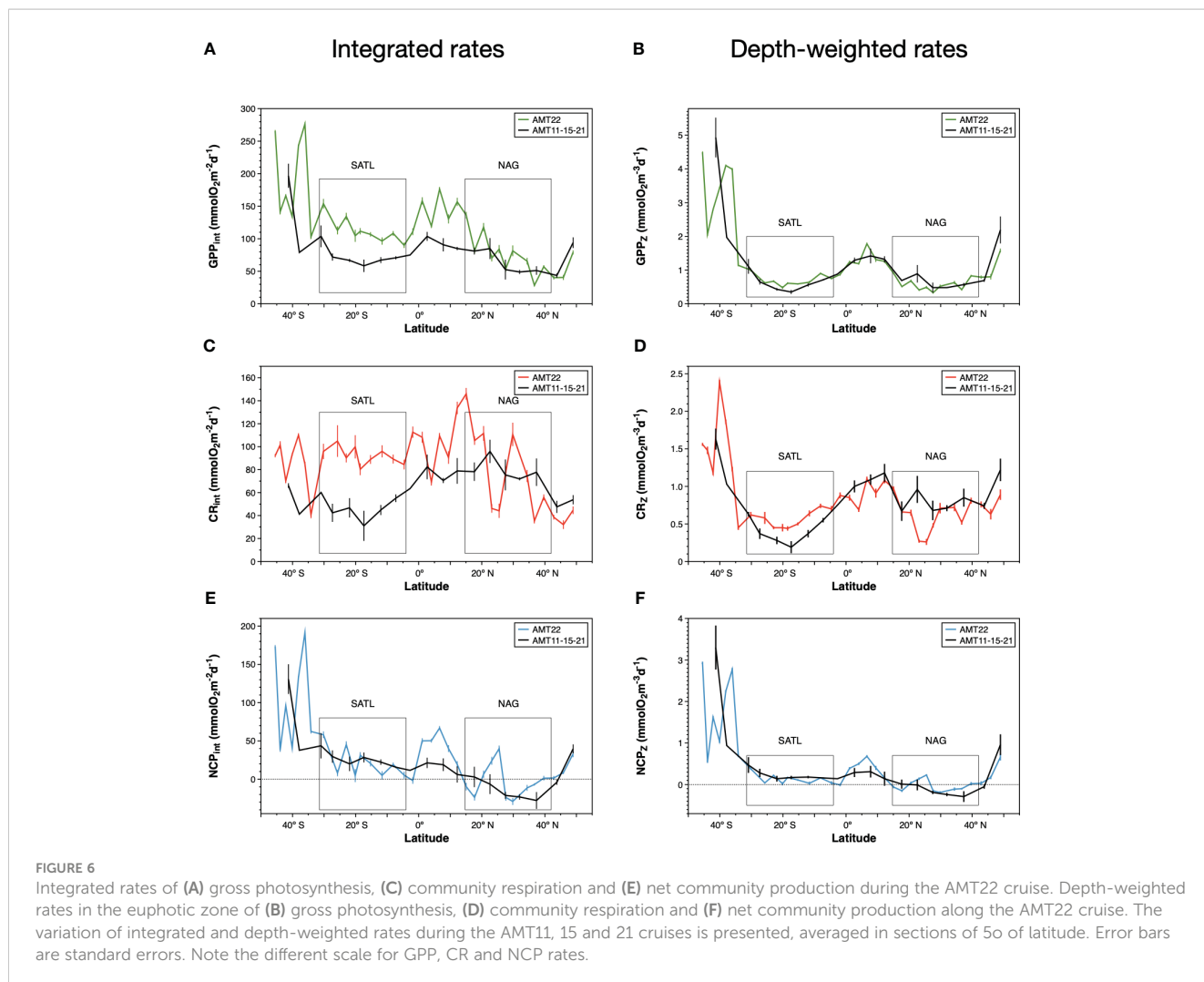
reflect on differences in phytoplankton composition and community structure (see above). This strong relationship allows the estimation of a general daily assimilation number (ratio of photosynthetically O_2 produced per mg Chla per day) of $4.35 \text{ mmolO}_2 \text{ mgChla}^{-1} \text{ d}^{-1}$, which is near but below the maximum $5 \text{ mmolO}_2 \text{ mgChla}^{-1} \text{ d}^{-1}$ characteristic of oligotrophic systems (Karl et al., 2002; Marra et al., 2007; assuming 10 h of light and $\text{PQ}=1.1$) and agrees well with values measured during stratification periods

in coastal temperate ecosystems ($4.15 \pm 1.23 \text{ mmolO}_2 \text{ mgChla}^{-1} \text{ d}^{-1}$ in the Ría de Vigo during the summer; Lozano et al., 2021).

3.3.2 Community respiration

3.3.2.1 Volumetric rates

CR was less variable than GPP, ranging from $0.10 \pm 0.18 \text{ mmolO}_2 \text{ m}^{-3} \text{ d}^{-1}$ below the DCM in the central SATL to $3.51 \pm 0.20 \text{ mmolO}_2 \text{ m}^{-3} \text{ d}^{-1}$ near the surface at about 40° South (SSTC)



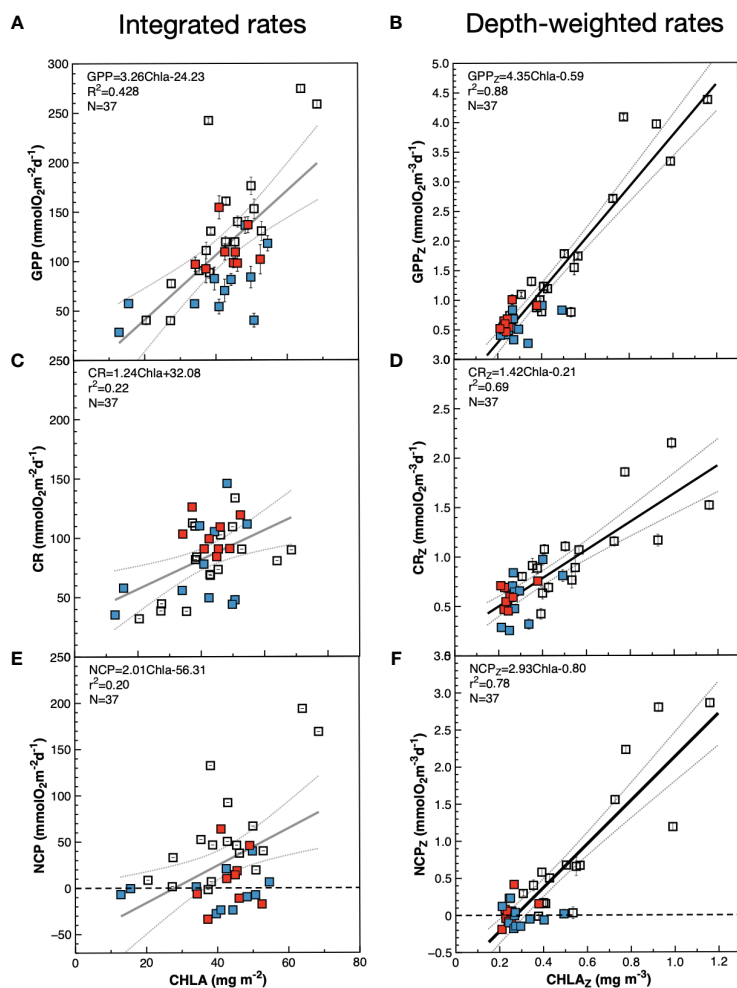


FIGURE 7

Relationships between chlorophyll a concentration and metabolic rates in the euphotic zone during the AMT22 cruise. Blue symbols are data from the NAG, red symbols are data from the SATL, open symbols are data from other provinces. (A, C, E), integrated values; (B, D, F), depth-weighted values calculated dividing the integrated values by the depth of integration (0.1% PAR depth). Results of general OLS regression analyses are always presented for comparison, despite the poor fit with integrated values (poorly fitted lines are presented in grey). The dotted lines are the 95% confidence interval. Error bars are standard errors.

(Figure 5). As with GPP, CR was high ($\geq 1 \text{ mmolO}_2 \text{ m}^{-3} \text{ d}^{-1}$) in the SSTC and also in the WTRA, particularly in its northern sector (approx. $15^\circ\text{-}5^\circ\text{N}$) above the DCM. However, in surface areas of the NADR with similar GPP and Chla values, low CR rates were observed. The lowest respiration was measured in the gyres, with values near $0.5 \text{ mmolO}_2 \text{ m}^{-3} \text{ d}^{-1}$ and very little depth or latitudinal variation through most of the S gyre. These values agree well with the SATL average of $0.48 \pm 0.02 \text{ mmolO}_2 \text{ m}^{-3} \text{ d}^{-1}$ in the AMT11-22 dataset (Table 1). The NAG showed similarly low depth variation, but higher latitudinal variation than the SATL, with very low CR rates (0.09 ± 0.15 to $0.45 \pm 0.13 \text{ mmolO}_2 \text{ m}^{-3} \text{ d}^{-1}$, average $0.25 \pm 0.03 \text{ mmolO}_2 \text{ m}^{-3} \text{ d}^{-1}$) in the central region of the gyre ($26\text{-}23^\circ \text{N}$) where high abundances of *Synechococcus* spp. were observed (see above). These low rates are less than half the CR measured elsewhere in the NAG ($>0.6 \text{ mmolO}_2 \text{ m}^{-3} \text{ d}^{-1}$), the latter agreeing with the average

NAG CR in the AMT11-22 dataset ($0.68 \pm 0.03 \text{ mmolO}_2 \text{ m}^{-3} \text{ d}^{-1}$; Table 1).

3.3.2.2 Integrated rates

The small range of volumetric CR is reflected in a weaker (if appreciable) regional variation of integrated CR (CR_{int}) compared to integrated GPP (Figures 6A, C; note differences in the Y scale). If any, lower CR_{int} was observed in the NADR and the NAG, although with too high a variation within this province to discern regional patterns. This would concur with the general agreement on the relative constancy of CR compared to GPP in the ocean (Karl et al., 2003; Williams et al., 2004; del Giorgio and Williams, 2005; Robinson and Williams, 2005; Carlson et al., 2007; Duarte et al., 2013; Regaudie-de-Gioux and Duarte, 2013). However, such a constancy partly results here from the regional differences in the

depth of the euphotic zone: when CR_{int} rates are divided by the depth of integration (0.1% PAR) a clear W-shaped latitudinal pattern emerges (Figure 6D), resembling the GPP_Z trend. Special attention deserves to be paid to the low CR region in the NAG at 26–23° N, which is clearly observable in both the volumetric, integrated and depth-weighted CR rates (Figures 5, 6). In addition to improved spatial patterns, CR_Z also markedly improves the relationship with Chla over the poor $Chla_{int} : CR_{int}$ relationship (Figures 7C, D).

3.3.3 Net community production and GPP: CR relationship

3.3.3.1 Volumetric rates

NCP ranged between $-1.50 \pm 0.16 \text{ mmolO}_2 \text{ m}^{-3} \text{ d}^{-1}$ near the bottom of the euphotic layer at 44° S, to $7.02 \pm 0.15 \text{ mmolO}_2 \text{ m}^{-3} \text{ d}^{-1}$ near the surface at about 45.5° S, both at the SSTC (Figure 5). NCP was $>0.4 \text{ mmolO}_2 \text{ m}^{-3} \text{ d}^{-1}$ in the Chla-rich, high GPP waters of the NADR, WTRA and SSTC. Strong vertical gradients of NCP developed in the periphery of the NADR and WTRA, where negative rates were measured in subsurface waters including the DCM. Low and mostly positive NCP was measured through the SATL (-0.48 ± 0.11 to $0.59 \pm 0.11 \text{ mmolO}_2 \text{ m}^{-3} \text{ d}^{-1}$, average $0.13 \pm 0.04 \text{ mmolO}_2 \text{ m}^{-3} \text{ d}^{-1}$), with very little vertical or latitudinal variation. A similar range was observed in the NAG (-0.43 ± 0.11 to $0.48 \pm 0.05 \text{ mmolO}_2 \text{ m}^{-3} \text{ d}^{-1}$), however, both the average ($-0.01 \pm 0.03 \text{ mmolO}_2 \text{ m}^{-3} \text{ d}^{-1}$) and distribution of NCP were different, with a general prevalence of net heterotrophy ($NCP < 0$) except throughout the euphotic zone at the low CR region in the central part of the gyre (26–23° N).

3.3.3.2 Integrated rates

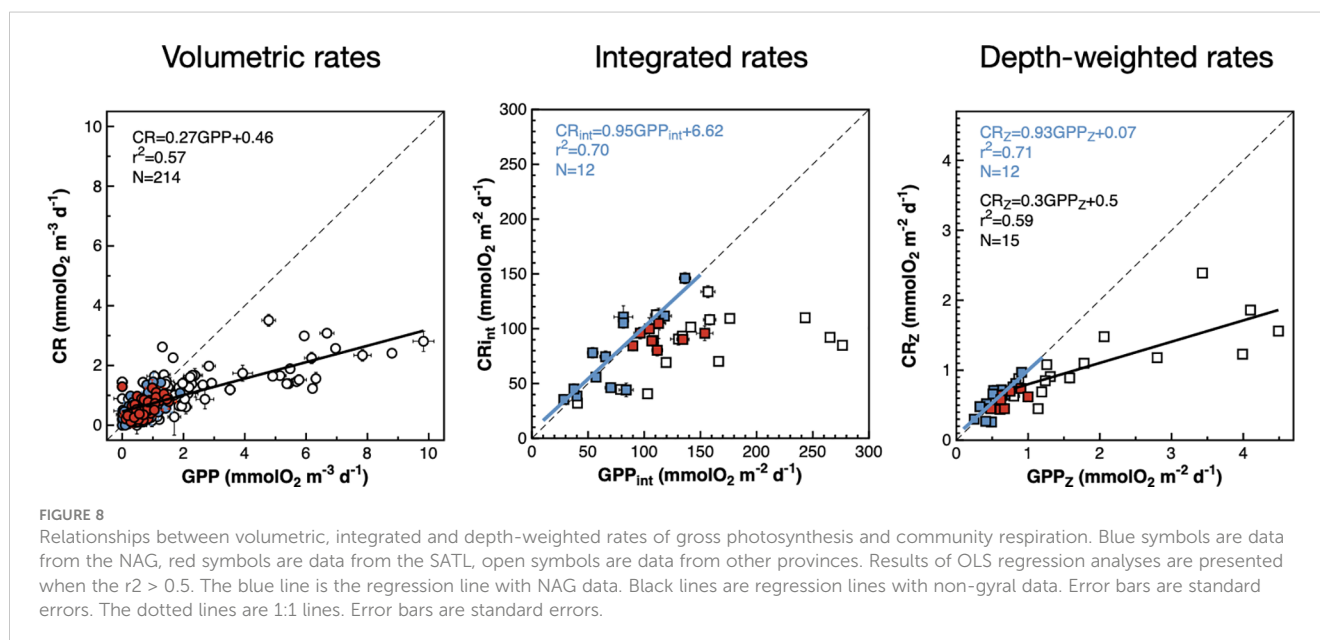
As with GPP and CR, depth-weighted NCP rates (NCP_Z) improve the representation of latitudinal patterns compared to integrated rates: the difference between the oligotrophic gyres and the productive provinces (especially the NADR) is increased, the difference between the two gyres is reduced and a W-shaped

latitudinal trend emerges (Figures 6E, F). Such a trend, which agrees with the latitudinal variation of the nitracline, is flattened compared to GPP_Z due to the enhanced respiration in the permanent upwelling systems of the WTRA, and asymmetric due to the lower NCP_Z in the NAG than in the SATL (caused by the higher CR_Z in the former). This NCP_Z trend also compares well with the average latitudinal variation of NCP_Z in the AMT11–15–21 dataset, and greatly improves the significance of the relationship of NCP with Chla (Figures 7E, F), with the average Chla in the euphotic zone ($Chla_Z$) explaining 78% of the variation of NCP_Z .

3.3.3.3 GPP: CR relationships

The depth and latitudinal covariation observed between volumetric and integrated CR and GPP rates during the AMT22 (Figures 5, 6) is reflected in significant GPP : CR relationships (Figure 8). Volumetric rates depict a single GPP : CR relationship, with no differences between mesotrophic and oligotrophic provinces, contrasting with different system-dependent relationships previously observed (Serret et al., 2009; Serret et al., 2015; Lozano et al., 2021). The generalised GPP : CR relationship has a slope < 1 and a threshold GPP for net heterotrophy ($GPP < CR$) of $0.63 \text{ mmolO}_2 \text{ m}^{-3} \text{ d}^{-1}$. This is a lower threshold than the $1.26 \text{ mmolO}_2 \text{ m}^{-3} \text{ d}^{-1}$ in Regaudie-de-Gioux and Duarte (2013), but would still predict net heterotrophy through extensive areas of the NAG and SATL where net autotrophy was observed (Figure 5), indicative of the poor predictive power of generalised relationships or derived thresholds between volumetric rates.

When integrated and depth-weighted rates are analysed, the GPP : CR relationships remain invariant for mesotrophic provinces (although a significant relationship is only observed with depth-weighted rates), but oligotrophic gyres showed a different behaviour: significant 1:1 $GPP_{int} : CR_{int}$ and $GPP_Z : CR_Z$ relationships were observed in the NAG, while results in the SATL did not show any significant trend. Although the different GPP : CR relationships between meso- and oligotrophic provinces agree with



previous observations (Serret et al., 2009), the relationships in the gyres disagree with observations in the AMT11-22 dataset, where a 1:1 relationship was observed in the SATL while the slope in the NAG was 0.76 (Serret et al., 2015). This conflict between the analysis of results from a single cruise and the meta-analysis of results from ten cruises over >10 years puts into question the scalability of the relationships and conclusions from such a meta-analysis and will be discussed in the next section.

3.4 Particulate ^{14}C primary production

The highest rates of particulate organic carbon production (^{14}CPP) were measured in the surface layer of the SSTC and, to a lesser extent, of the NADR and WTRA, and the lowest rates were measured in the SATL (Figure 9). In the productive temperate provinces, the vertical distribution of ^{14}CPP was tightly coupled to that of Chla, while in the equatorial upwelling province (WTRA) and in the stratified oligotrophic gyres, ^{14}CPP was always higher near the surface, detached from the deep maxima in Chla and nano- and picophytoplankton abundances. Higher rates were observed in the NAG than in the more oligotrophic SATL.

The depth and latitudinal variation of ^{14}CPP and O_2 GPP were very similar. The relationship between GPP and ^{14}CPP is described by the equation $\text{GPP} (\text{mmolO}_2 \text{ m}^{-3} \text{ d}^{-1}) = 1.83^{14}\text{CPP} (\text{mmolC m}^{-3} \text{ d}^{-1}) + 0.42$, $n = 198$, $r^2 = 0.88$, $p < 0.01$, which agrees with the 1.94 slope observed in the AMT11 dataset (Serret et al., 2006) and with the results in Bender et al. (1999) where 24-h ^{14}CPP rates were ca. 45% of O_2 GPP in the equatorial Pacific, but are lower than the GPP to ^{14}CPP ratio of 7.1 ± 0.1 in the meta-analysis of Regaudie-de-Gioux and Duarte (2013). Excluding negative values, the relationship of net community production (NCP) with ^{14}CPP is described by the equation $\text{NCP} (\text{mmolO}_2 \text{ m}^{-3} \text{ d}^{-1}) = 1.3^{14}\text{CPP} (\text{mmolC m}^{-3} \text{ d}^{-1}) + 0.07$, $n = 135$, $r^2 = 0.70$, $p < 0.01$, which is between the theoretical photosynthetic quotients of 1.4 ± 0.1 and 1.1 ± 0.1 for new and recycled production (Laws, 1991), and concurs with the 1.4 slope obtained by Marra (2009) from the regression between ^{14}C assimilation and O_2 NCP data from 4 JGOFS process studies.

Picophytoplankton was the size-fraction dominating the photosynthetic production of particulate carbon throughout the transect, followed by the nanoplankton (Figure 9). The relative contribution of the nanoplankton to total ^{14}CPP was higher near the surface and decreased markedly with depth in the gyres, reaching <20% at the DCM. The contribution of the picophytoplankton was higher at depth, particularly in the gyres, where it represented >60% throughout the DCM and reached >80% especially in the SATL. A marked decrease in the percentage of ^{14}CPP by the picoplankton was observed near the centre of the NAG (at around 25°N), just below the layer where high numbers of *Synechococcus* spp. cells were observed together with reduced CR rates. Such a decrease resulted from an almost five times increase in the rate of ^{14}CPP by cells $>10 \mu\text{m}$, reaching $121.74 \pm 18.06 \text{ mgC m}^{-2} \text{ d}^{-1}$ (vs. a regional average, excluding this station, of $25.04 \pm 16.14 \text{ mgC m}^{-2} \text{ d}^{-1}$). Despite the relative importance, overall range and regional variation of the percentage of ^{14}CPP by the

picophytoplankton, no relationship was observed with either GPP, CR or the GPP/CR ratio (Figure 10).

4 Discussion

Community respiration is a relatively slow variable that integrates the energy-producing process that supports the maintenance, activity and growth of most auto- and heterotrophic organisms in the oxygenated ocean. All three components of respiration depend on the availability of organic matter, which should reflect on tight relationships between CR and the biomass and production of autotrophic organisms (Robinson and Williams, 2005). However, the faster response of photosynthesis to environmental forcing implies that photosynthesis and respiration are not always tightly connected, especially at the community level and in the dynamic ocean. Sinking, trophic processes (e.g., lability or stoichiometric constraints on heterotrophy), or community dynamics (e.g., different population growth or loss rates of auto- and heterotrophs) mean that, even in a theoretically isolated water column, the respiration of organic matter may occur with some delay or deeper than when/where it was produced. To cope with these differences in scale, Williams (1998) proposed to use depth-integrated GPP and CR rates to obtain “a more accurate picture of the distribution of the balance of autotrophy and heterotrophy in the oceans”. Integrated values are certainly useful when we are interested in pooled balances (e.g., the bulk net production of a region summarizes the total amount of organic matter available for export to depth or transfer to higher trophic levels). However all trophic processes require the interaction between particles, which depends on encounter rates that are governed more by concentration than areal magnitude (e.g., nitrate uptake kinetics, DOM respiration or predation). Hence, depth-weighted values (which represent average concentrations or rates) not only improve the comparison between regions differing largely in euphotic depth, but they also provide a more accurate representation of the interaction between fast and slow trophic processes across the whole layer of interest. Our results confirm that both the representation of the distribution of the balance of autotrophy and heterotrophy in the oceans, and the relationships between plankton metabolism and environmental variability across different ecosystems improve when a) the surface layer of interest reaches from the surface to the depth of 0.1% PAR ($Z_{0.1\% \text{PAR}}$) and b) depth-weighted, rather than volumetric or integrated values are used.

4.1 The euphotic zone depth for GPP and CR interaction is the depth of 0.1% PAR

Based on calculations of the compensation depth, Marra et al. (2014) found that the base of the euphotic zone was consistently deeper than the 1%PAR ($Z_{1\% \text{PAR}}$), and concluded that it occurs “at a depth that encompasses the depth range of all, or nearly all, autotrophic biomass”. In our study, the depth encompassing

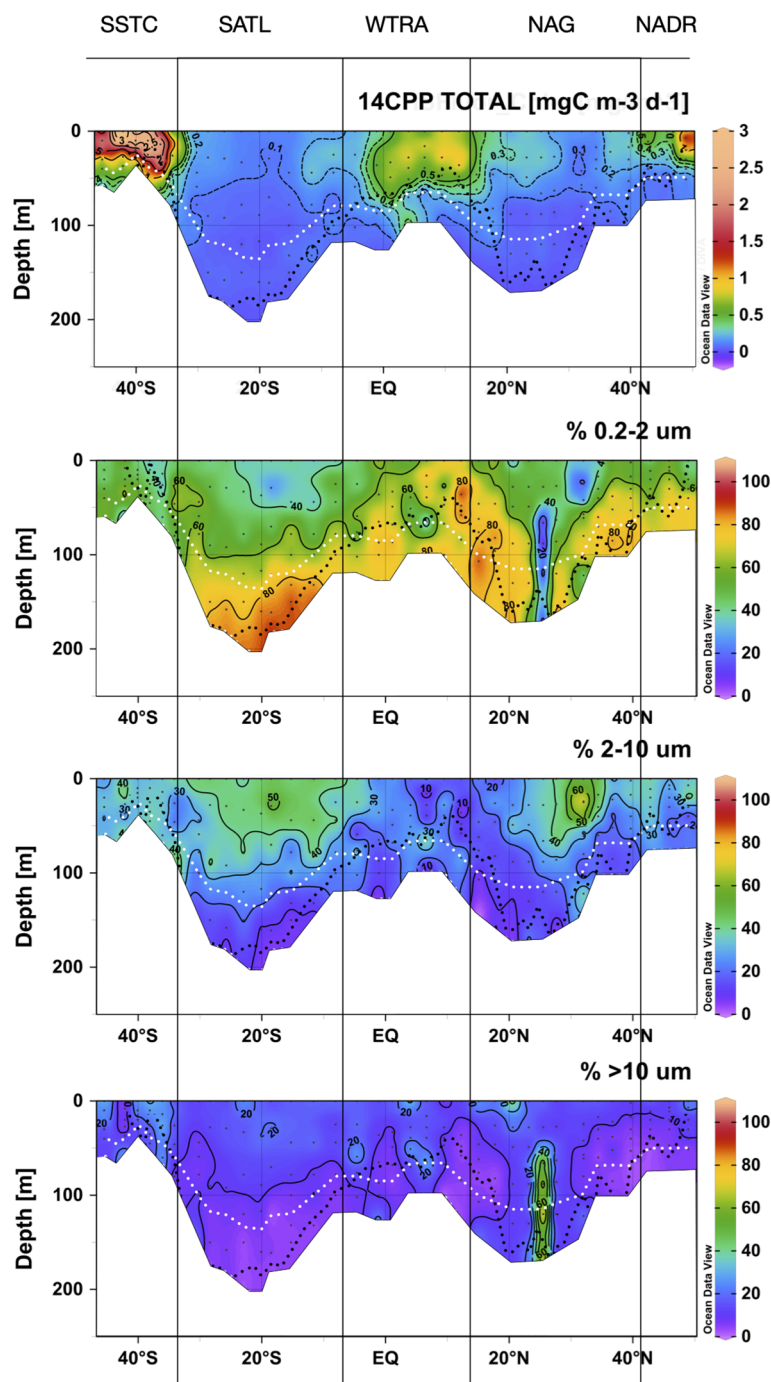
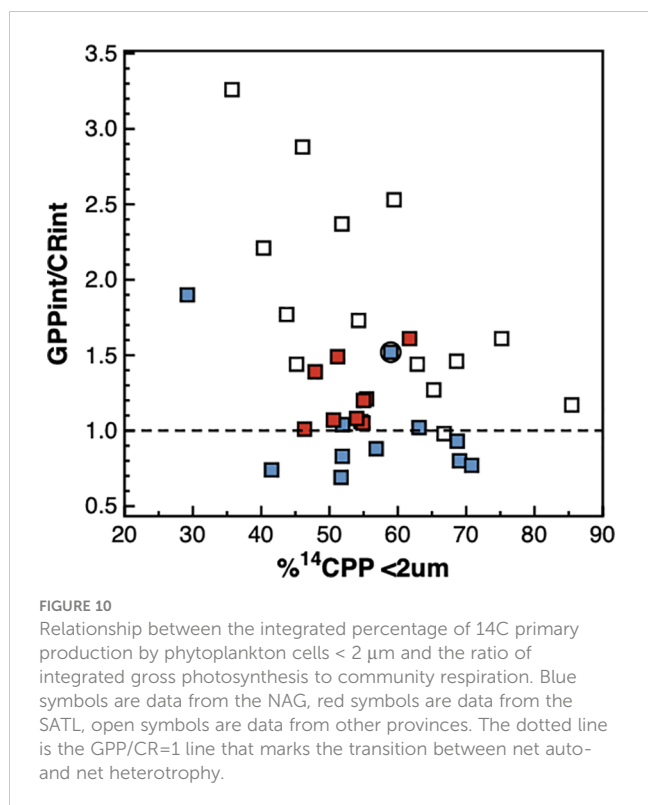


FIGURE 9

Depth vs. latitude sections of total and size-fractionated ^{14}C primary production during the AMT22 cruise. The white dotted lines are the depths of the 1 and 0.1%PAR. The black dotted line is the depth of the nitracline. The blanked area is the location of the deepest sample of each profile, at the depth of the 0.1%PAR. The approximate location of biogeographic provinces (Longhurst, 1998) is presented. Figures produced using Ocean Data View (Schlitzer, Reiner, Ocean Data View, <https://odv.awi.de>, 2022).

nearly all Chla is $Z_{0.1\%PAR}$ (see Figure 3), where average GPP was 0.18 ± 0.09 and 0.30 ± 0.06 $\text{mmolO}_2 \text{m}^{-3} \text{d}^{-1}$ in the NAG and SATL, respectively. Moreover, the biological depletion of nitrate in both the NAG and SATL reached depths exceeding the $Z_{1\%PAR}$, so that the nitracline was up to 50 m deeper, near the $Z_{0.1\%PAR}$. All this confirms that the $Z_{1\%PAR}$ is too shallow a boundary for the euphotic zone, which agrees with the observations of Laws et al. (1987) in the

N Pacific gyre, where the contribution of photosynthesis below the $Z_{1\%PAR}$ to integrated rates was estimated to be 14%. In a recent comprehensive meta-analysis of optical and biological determinants of the euphotic zone depth, Wu et al. (2021) concluded that the depth of $Z_{1\%PAR}$ is often too shallow compared to the compensation depth, but also found that the $Z_{0.1\%PAR}$ was too deep. This, however, reinforces our conclusion because Wu et al. (2021) identified the



base of the euphotic zone with the compensation depth, “where the rate of photosynthesis equals that of autotrophic respiration, that is, $\text{NPP} = 0$ ”. Our interest in community metabolic balances (GPP and CR) justifies the extension of the euphotic zone to the deeper layer where GPP (rather than NPP) becomes undetectable, with the $Z_{0.1\% \text{PAR}}$ as a reliable proxy.

4.2 The variation of CR_Z in the oligotrophic ocean is systematic and relevant for the metabolic state

The existence of important differences in $Z_{0.1\% \text{PAR}}$, both between and within provinces, produces some biases or difficult to understand patterns of integrated community metabolism (e.g., higher GPP_{int} in the oligotrophic NAG than in the mesotrophic NADR, higher CR_{int} in the low biomass NAG than in the high biomass SSTC. Figure 6), which are cancelled out when the integrated rates are divided by their respective depth of integration. CR_Z and GPP_Z , which are the average rates through the euphotic zone, compensate potential transient/local imbalances in volumetric rates caused by the different scale of the relatively fast photosynthesis and the relatively slow respiration. Hence, they concur with integrated rates at providing a better representation of the plankton community metabolic interactions and balances (Williams, 1998), while avoiding the bias caused by regional differences in depth of integration. The use of depth-weighted rates produces sensible latitudinal W-shaped patterns of GPP, in line with the variation of nutrient availability in the euphotic zone (see Results). More importantly, it produces the emergence of

unusually clear CR patterns that were blurred by the biased spatial variability of CR_{int} (Figure 6). The asymmetric W-shaped latitudinal variation of CR_Z compares very well with the average CR_Z trend in the AMT11-15-21 dataset, and with the higher average CR in the NAG than in the SATL in Serret et al. (2015) (Table 1). This suggests that these are characteristic, biogeographic, features of the Atlantic Ocean, which challenges the minor importance attributed to CR on the variation of metabolic balances in the oligotrophic ocean. Such irrelevance is based on the observation of a relative constancy of CR compared to the large variation of primary productivity (Karl et al., 2003; Williams et al., 2004; del Giorgio and Williams, 2005; Robinson and Williams, 2005; Carlson et al., 2007; Duarte et al., 2013; Regaudie-de-Gioux and Duarte, 2013). We conclude that such relative constancy partly resulted from the analysis of volumetric or integrated rates. Our results show that the variation of CR_Z in the oligotrophic ocean is systematic and relevant for regional patterns of NCP_Z , implying that the variation of NCP cannot be determined from the variation of GPP alone (as in e.g. Westberry et al., 2012; Duarte et al., 2013).

4.3 CR_Z covaries with Chl_Z over the Atlantic Ocean

Significant volumetric and integrated GPP : CR relationships have often been obtained (Robinson and Williams, 2005; Regaudie-de-Gioux and Duarte, 2013; Serret et al., 2015, and references therein) and used to predict NCP at regional-global scales (e.g., Duarte and Agusti, 1998; Westberry et al., 2012). As heterotrophic respiration is supported by autotrophic biomass, not by GPP, and biomass is a slower variable than GPP, one would expect stronger Chl_a : CR relationships. However, individual studies and meta-analyses have failed to obtain significant empirical evidence of a relationship of CR with total Chl_a , or with the autotrophic community structure. For instance, of the 18 individual studies analysed by Robinson and Williams (2005), in only 50% was the r^2 of the Chl_a : CR relationship greater than 0.3, and these were studies in shelf seas with ranges of Chl_a ($0.2\text{--}50 \text{ mg m}^{-3}$) and CR ($1\text{--}53 \text{ mmolO}_2 \text{ m}^{-3} \text{ d}^{-1}$) that are 18 and 17 times larger than our open ocean ranges. The meta-analysis of Regaudie-de-Gioux and Duarte (2013) obtained a similarly poor relationship ($R^2 = 0.29$, $p < 0.05$) with the 1111 pairs of data included. And the recent review of processes regulating CR by Wikner et al. (2023) reported only two significant Chl_a : CR relationships, both based on integrated values in coastal embayments with very large magnitude and variability of Chl_a and CR (Smith and Kemp, 2001, Chesapeake Bay; Olesen et al., 1999, Gulf of Riga -although Figure 9 in the latter puts into question the consistency of this relationship). Altogether, the very little evidence on the influence of Chl_a on plankton respiration leads to Chl_a being not included or removed from empirical models of CR (Wikner et al., 2023), which undermines the potential for the Earth observation of CR. Our volumetric and integrated CR and Chl_a data concur with this lack of relationship (the r^2 of the Chl_{int} : CR_{int} relationship was 0.22, agreeing with previous studies), however, a significant relationship emerges when depth-weighted data are analysed ($\text{CR}_Z = 1.42 \text{Chl}_Z - 0.21$, $r^2 = 0.69$, $N = 37$, $p < 0.001$)

(Figure 7). Given the paucity of previous observations, this is an important result with potential for the difficult prediction of CR from a variable that can be estimated remotely. A general ratio of $1.42 \text{ mmolO}_2 \text{ mgChla}^{-1} \text{ d}^{-1}$ can be tentatively proposed for the Atlantic, although further analyses of spatial and temporal variation are necessary (note that all our observations were made during the boreal autumn). From the x-intercept of the significant $\text{Chla}_Z : \text{NCP}_Z$ relationship (Figure 7), a threshold Chla for net heterotrophy of ca. $0.25 \text{ mgChla m}^{-3}$ can be derived. This is lower than the $0.35 \text{ mgChla m}^{-3}$ in Regaudie-de-Gioux and Duarte (2013), thus reducing the magnitude of extrapolated heterotrophy in the global open ocean, although such a threshold is a broad generalization, not useful for actual prediction of metabolic rates in specific communities.

4.4 Revisiting meta-analysis of AMT data

The practical value of using depth-weighted rates is further evidenced by the examination of the disagreement between the variation of metabolic rates in the AMT22 vs. the AMT11-22 datasets, which puts into question the validity of the GPP : CR relationships in Serret et al. (2015) to represent and predict the actual variation of NCP in the oligotrophic Atlantic (see section 3.3.3.3 above). The combined AMT11-22 dataset depicted differences in average NCP and in the $\text{GPP}_{\text{int}} : \text{CR}_{\text{int}}$ relationship between the two gyres (slopes were 1 in the SATL and 0.7 in the NAG) indicative of the prevalence of heterotrophy only in the NAG, which agrees with its higher liability to inputs of allochthonous organic matter (e.g., Reynolds et al., 2014). No such differences exist in the AMT22 dataset: average NCP was not negative in either the SATL or the NAG, and average GPP_Z and CR_Z rates were not significantly different between the NAG and SATL (GPP_Z : t-Value=1.58, df=19, P=0.13; CR_Z : t-Value=0.28, df=19, P=0.78) (Table 1); moreover, a 1:1 GPP : CR relationship was observed only in the NAG (P<0.001) (Figure 8). The analysis of integrated rates would indicate that the cause for such a

disagreement in the NAG was its higher GPP_{int} in the AMT22, as average CR_{int} remained invariant (Table 1). However, depth-weighted rates, which are pertinent because integration in Serret et al. (2015) only reached the $Z_{1\% \text{PAR}}$ vs. $Z_{0.1\% \text{PAR}}$ here, shows that it was average GPP_Z that remained invariant and the unusual metabolic balance in the NAG was due to the lower than usual average CR_Z rates in the AMT22 compared to the AMT11-22 series (Table 1; Figure 6).

A closer inspection shows however, that, except at the low CR region in the central part of the gyre (26-23° N), negative NCP did actually prevail through the NAG (Figures 5, 6), agreeing with both the regional average in Serret et al. (2015) and with the latitudinal variation in the spatially coherent AMT11-15-21 subset. Such a locally anomalous region is the cause of the disagreements in the NAG presented above: the average NCP_{int} and NCP_Z in the NAG outside that region are $-12.17 \pm 3.69 \text{ mmolO}_2 \text{ m}^{-2} \text{ d}^{-1}$ and $-0.08 \pm 0.02 \text{ mmolO}_2 \text{ m}^{-3} \text{ d}^{-1}$, respectively, not different to the NAG averages in Serret et al. (2015) (Table 1). And the $\text{GPP}_Z : \text{CR}_Z$ relationship excluding the two anomalous data from 26-23° N is the same as the autumn NAG equation in Serret et al. (2015) (Figure 11). This exception thus actually confirms the general validity of the GPP : CR relationships from the aggregated AMT11-22 data at ecologically relevant scales.

4.5 Phytoplankton size-structure does not regulate the relationship and balance of GPP and CR

Such a region of anomalously low CR and positive NCP coincided with the area of anomalously high abundance of *Synechococcus* spp. and >4 times increase in ^{14}CPP by cells >10 μm ($^{14}\text{CPP}_{>10}$). This agrees with conceptual and mechanistic models that highlight the role of phytoplankton size in the organisation of aquatic food webs (Legendre and Le Fevre, 1989; Kiørboe, 1993). These models emerge from the cell size-dependency of factors regulating growth and loss rates of phytoplankton

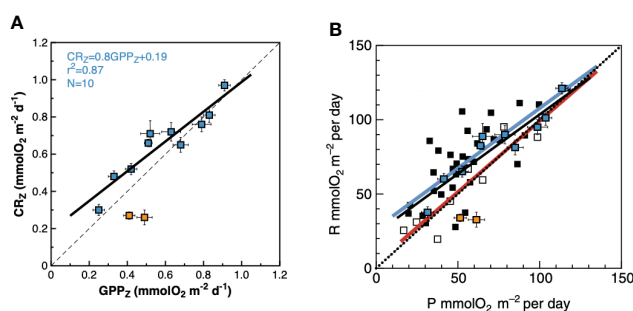


FIGURE 11

Relationship between the depth-weighted rates of gross primary production and community respiration in the N Atlantic gyre. (A) AMT22 data. Orange squares are the data from 26-23° N; blue squares are the rest of the data in the NAG. Results of OLS regression analysis with data outside the 26-23° N region are presented. See text for details. The dashed line is the 1:1 line that marks the transition between net auto- and net heterotrophy. (B) AMT22 data and regression line (black line) overlaid on Figure 7A of Serret et al. (2015), depicting the relationship between the integrated rates of gross primary production and community respiration in the NAST and SATL in autumn (coinciding with the time of the year of the AMT22 cruise). The blue line is the regression line for the NAST data: $\text{CR} = 0.80\text{GPP} + 26.9$, $R^2 = 0.54$, $n = 33$. The red line is the regression line for the SATL data: $\text{CR} = 0.96\text{GPP} + 3.56$; $R^2 = 0.87$; $n = 9$. The dotted line indicates the 1:1 line. Error bars are standard errors.

populations (competitive advantage for light or nutrients, photosynthetic efficiency, sinking or grazing rates). The size selectivity of predators for prey would then shape the size structure of the entire food web, causing that transitions in the relative importance of trophic pathways (from the herbivorous food web to the microbial loop) are ultimately controlled by the relative dominance of large vs. small phytoplankton (e.g., Finkel, 2007 and references therein). According to this paradigm, the relationship between GPP and CR would be largely regulated by the size structure of the community, so that higher GPP : CR ratios and NCP rates are expected in communities dominated by large phytoplankton and herbivorous food webs (Smith and Kemp, 2001). These expectations are met in the comparison of the patch of high $^{14}\text{CPP}_{>10}$ at 23–26 °N with the rest of the NAG, although the high GPP : CR ratios (1.9) and positive NCP_Z were not accompanied by concurrent increases in either Chla, total ^{14}CPP or GPP, but resulted entirely from a marked decrease in CR_Z (Figure 6). These results confirm the relevance of the variation of CR_Z in the oligotrophic ocean, not only for the regional differences in metabolic state (see above), but also for local/transient variations of NCP_Z driven by changes in community structure within provinces. This evidences the importance of improving the parameterisation of respiration for realistic projections of the biological carbon pump. The significant CR_Z : Chla_Z relationship observed here (see above) and the sharp change in CR_Z associated with a patch of high *Synechococcus* spp. abundance and $^{14}\text{CPP}_{>10}$ indicate that the biomass and structure of phytoplankton communities are important overlooked parameters regulating CR that need to be incorporated in predictive models.

A wider analysis however disputes the generality of the relationship between phytoplankton size and the degree of heterotrophy predicted by food web models. These models have been mostly validated based on the relative abundances and growth rates of different trophic compartments (e.g., Armengol et al., 2019), size fractionated primary production and autotrophic biomass (e.g., Tremblay and Legendre, 1994) or vertical flux of particles (e.g., Guidi et al., 2009). However, there is very little empirical confirmation of a relationship between direct measurements of the energy transfer efficiency or the degree of heterotrophy (e.g. GPP : CR ratio) and the phytoplankton size-structure, and only in coastal embayments and strong transition zones, and with unclear results (Serret et al., 2001; Smith and Kemp, 2001; Arbones et al., 2008; Soria-Piriz et al., 2017; Wang et al., 2018; Juranek et al., 2020; Lozano et al., 2021). Such a relationship is an important validation for these models because it does not entail the improbable assumption that population and energy dynamics are tightly connected over nested spatial and temporal scales in the non-steady state pelagic ecosystem. Our AMT22 results show no significant relationship between GPP : CR ratios and the percentage of ^{14}CPP in any size fraction. Within a given $\%^{14}\text{CPP}_{<2}$ between ~40 and 70%, the full range of GPP : CR ratios can be observed; while the same value of the GPP : CR ratio may be observed through the full range of $\%^{14}\text{CPP}_{<2}$ (Figure 10). More significantly, a biogeographic pattern emerges from this relationship: at any $\%^{14}\text{CPP}_{<2}$, the lowest GPP : CR ratios were always observed in the NAG, intermediate values were

observed in the SATL, and the highest GPP : CR ratios were always observed in mesotrophic provinces (Figure 10). This all indicates that the phytoplankton size structure is a poor predictor of regional differences in the functioning of food webs and in the trophic state of the pelagic ecosystem. This spatial analysis of variation concurs with the temporal observations of Lozano et al. (2021) over a twice-monthly seasonal study in the temperate coastal upwelling system of the Ría de Vigo. Results there only conformed to predictions of models when highly contrasting situations were compared (the highly autotrophic microphytoplankton-dominated upwelling vs. the almost in balance pico- and nanophytoplankton-dominated winter mixing period), similar to the comparison of AMT22 data from the contrasting 26–23° N patch vs. the rest of the N gyre. However, both the AMT22 dataset and the seasonal variation in the Ría de Vigo revealed the absence of a systematic relationship between phytoplankton size and the degree of heterotrophy, thus refuting the hypothesis that cell size determines food web functioning. This also agrees with observations of high NCP in communities dominated by small phytoplankton in the Southern Ocean (Cassar et al., 2015) and tropical estuaries (Soria-Piriz et al., 2017), and with the weak relationship between taxonomy and NCP in low-production waters of the NW Atlantic (Wang et al., 2018). The idea that higher respiration per unit biomass or primary production should occur in a consumer-controlled and complex microbial food web where heterotrophic activities and remineralisation play key roles for the maintenance of the community, and the biomass of heterotrophs exceeds that of autotrophs (Gasol et al., 1997), than in simpler, resource-controlled herbivore food webs, seems irrefutable (Legendre & Le Fevre, 1989; Kiørboe, 1993; Legendre & Rassoulzadegan, 1996). However, our results show that such a theoretical connection is not always realised in the ocean, either because it is short-circuited by the differences in scale between population and trophic dynamics, or because other size-independent processes regulating GPP or CR have a larger impact on community metabolism patterns (for instance the higher inputs of allochthonous organic matter in the NAG, e.g., Reynolds et al., 2014; Serret et al., 2015).

4.6 Alternative ecosystem states constrain prediction of NCP in the upper ocean

The discussion above highlights the importance of the biogeographic component in the variation of plankton CR and NCP in the Atlantic Ocean, agreeing with the system dependency observed in ^{14}CPP : NCP relationships (Serret et al., 2009). These are potentially useful relationships for prediction, because of the methodological independence of the variables and the large global dataset of ^{14}CPP measurements and Earth observation algorithms. Two such distinct models in the Atlantic represented productive +isolated oligotrophic ecosystems (AMT11 model) and productive +subsidised oligotrophic ecosystems (AMT6 model), respectively (for details, see Serret et al., 2009). To explore the consistency of this spatial partition, we have analysed the seasonal variation in the Ría de Vigo in Lozano et al. (2021), where two distinct periods were

identified: winter-spring, when heterotrophy was locally sustained by relatively low productive situations, thus resembling the AMT11 model; and summer, when episodes of strong organic matter accumulation driven by short upwelling events were followed by periods of stratification and increased heterotrophy representing temporally subsidised oligotrophic systems similar to those in the AMT6 spatial model. The striking similarity observed in the ¹⁴CPP : NCP relationships in donor- (AMT6, summer upwelling) vs. locally controlled ecosystems (AMT11, winter spring) across the Atlantic Ocean and through the year in the Ría de Vigo (Figure 12A) is a robust validation of the system dependency of empirical relations of community metabolism, and confirms that NCP can be accurately predicted in the ocean. However, such prediction remains challenging in practice, because our poor knowledge on respiration variation and control implies that determining which

system-dependent relationship will suit a particular ecosystem is difficult. For instance, the AMT22 dataset included oligotrophic data from the remote SATL (as the AMT11 model), but also included data from the supposedly subsidised NAST-E (as the AMT6 model). Yet the AMT22 ¹⁴CPP : NCP relationship including all these data tightly corresponds to the AMT11 model only (Figure 12B), which agrees with the unusual GPP : CR relationship and overall metabolic balance observed in the NAG during the AMT22 (see above). Even for the region of the open ocean whose metabolic balance has been more thoroughly studied (the NAST-E; see Regaudie-de-Gioux and Duarte, 2013 and Serret et al., 2015), prediction of NCP at ecological scales remains elusive because of the difficulty to determine which empirical model to use.

The persistence of distinct GPP : CR and ¹⁴CPP : NCP relationships within types of ecosystems, and the independence of

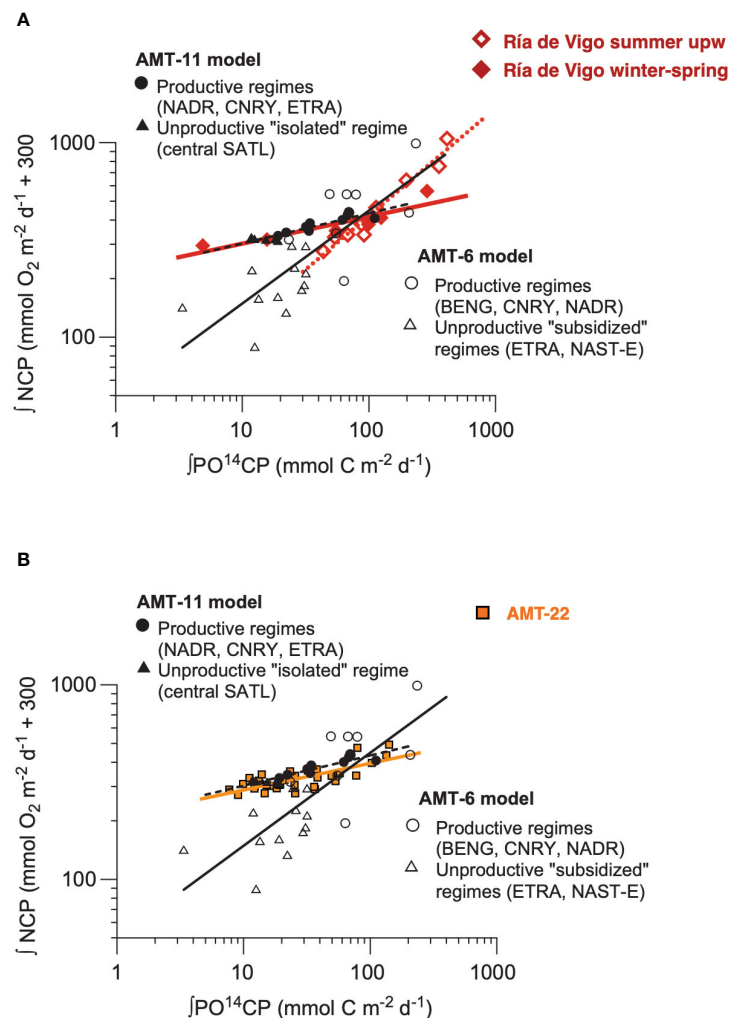


FIGURE 12

Relationship between the integrated rates of ¹⁴C primary production and net community production in (A) a seasonal study in the Riia de Vigo (Lozano et al., 2021) (red symbols and lines) and (B) the AMT22 (orange squares and line), both overlaid on Figure 2 from Serret et al. (2009) for comparison with the AMT6 (open symbols and black continuous line) and AMT11 (black filled symbols and black dashed line) models from Serret et al., 2009. The red continuous line is the OLS regression line with the winter-spring data in the Riia de Vigo ($^{14}\text{CPP}_{\text{int}} = 0.80\text{GPP} + 26.9$, $R^2 = 0.54$, $n = 33$). The equations are $\text{NCP}_{\text{int}} = 212.0114\text{CPP} - 300$, $r^2 = 0.85$, $n = 15$, $p < 0.001$ (AMT11, black dashed line), $\text{NCP}_{\text{int}} = 49.5314\text{CPP} - 300$, $r^2 = 0.61$, $n = 21$, $p < 0.001$ (AMT6, black continuous line), $\text{NCP}_{\text{int}} = 219.2014\text{CPP} - 300$, $r^2 = 0.82$, $n = 6$, $p < 0.001$ (Riia de Vigo, winter-spring, red continuous line), $\text{NCP}_{\text{int}} = 33.0314\text{CPP} - 300$, $r^2 = 0.95$, $n = 9$, $p < 0.001$ (Riia de Vigo, summer, red dotted line), and $\text{NCP}_{\text{int}} = 209.1614\text{CPP} - 300$, $r^2 = 0.58$, $n = 35$, $p < 0.001$ (AMT22, orange continuous line).

community metabolism from the size-structure of the phytoplankton evidence the existence of alternative ecosystem states (e.g., Holling, 1973; Beisner et al., 2003; Carpenter et al., 2022) emerging from a trophic resilience that overcomes regional and seasonal differences in community composition and structure in the upper ocean. This implies that strong perturbations of the community structure are necessary to shift the trophic functioning (e.g., at 26–23° N during the AMT22, during upwelling in the Ría de Vigo), which reflects on the observed lack of a general relationship between the degree of heterotrophy and the phytoplankton size (Lozano et al., 2021, this work) or taxonomic composition (Wang et al., 2018). On the other hand, a biogeographic perspective emerges from the responsiveness of state variables (such as the metabolic state and the GPP : CR relationships) to changes in environmental parameters (such as inputs of allochthonous organic matter or the dynamics of inorganic nutrients) that vary systematically between regions and along seasons. Identifying which are all those meaningful parameters and how they vary in the ocean would allow one to define domains for NCP prediction just as biogeographic provinces are used to define domains for PP models (e.g., Longhurst, 1998). In these models, photosynthetic parameters are assigned “on the basis of ecological provinces of the ocean” (Kulk et al., 2020), classified based on the hydrodynamic conditions, supply of nutrients and average irradiance. An analogous biogeography based on CR regulation is necessary to develop a global NCP prediction that is urgently needed for projections of carbon storage in a changing ocean. The system-dependency of empirical models is a suitable tool to identify some domains for NCP prediction, but global prediction requires understanding trophic resilience and determining thresholds for transitions between alternative ecosystem states, which demands a better knowledge of the processes regulating community metabolism in the ocean (especially CR) and their interaction with both community organisation and the variation of environmental parameters. This calls for a very substantial improvement of the global dataset of reliable measurements of plankton metabolism in the euphotic zone.

Data availability statement

The original contributions presented in the study are included in the article/Supplementary Material. Further inquiries can be directed to the corresponding author. The complete data set of all the physical, chemical and biological variables is available at the British Oceanographic Data Centre (<http://www.bodc.ac.uk/projects/uk/amt>). The conditions under which the data may be used are in line with the NERC Data Policy (<http://www.nerc.ac.uk/research/sites/data/policy/>), and will be explained following a request, before the delivery of data.

References

Arbones, B., Castro, C. G., Alonso-Perez, F., and Figueiras, F. G. (2008). Phytoplankton size structure and water column metabolic balance in a coastal

Author contributions

PS conceptualized this study, analyzed the results and wrote the manuscript, which was reviewed and edited by coauthors. PS and JL measured plankton metabolism. CH and EMSW provided the nutrients data. PL and GHT provided the ¹⁴CPP data. GAT and MZ provided cell counts data. All authors contributed to the article and approved the submitted version.

Funding

The Atlantic Meridional Transect is funded by the UK Natural Environment Research Council through its National Capability Long-term Single Centre Science Programme, Climate Linked Atlantic Sector Science (grant number NE/R015953/1). This study contributes to the international IMBeR project and is contribution number 398 of the AMT programme. The Spanish MICINN grant Scaling, monitoring and predicting marine plankton metabolism in a changing ocean CTM2011-29616 awarded to PS partly funded this study.

Acknowledgments

We thank all personnel on board during the AMT22 cruise (RRS James Cook JCO79). Special thanks to Rob Thomas for chlorophyll a measurements used to calibrate the CTD fluorescence sensor. We acknowledge the comments by the reviewers, which improved the paper.

Conflict of interest

The authors declare that the research was conducted in the absence of any commercial or financial relationships that could be construed as a potential conflict of interest.

The handling editor VB declared a past collaboration with the authors EMSW and GHT.

Publisher's note

All claims expressed in this article are solely those of the authors and do not necessarily represent those of their affiliated organizations, or those of the publisher, the editors and the reviewers. Any product that may be evaluated in this article, or claim that may be made by its manufacturer, is not guaranteed or endorsed by the publisher.

upwelling system: the Ría de Vigo, NW Iberia. *Aquat. Microb. Ecol.* 50, 169–179. doi: 10.3354/ame01160

- Armengol, L., Calbet, A., Franchy, G., Rodríguez-Santos, A., and Hernández-León, S. (2019). Planktonic food web structure and trophic transfer efficiency along a productivity gradient in the tropical and subtropical Atlantic ocean. *Sci. Rep.* 9, 2044. doi: 10.1038/s41598-019-38507-9
- Behrenfeld, M. J., and Falkowski, P. G. (1997). Photosynthetic rates derived from satellite-based chlorophyll concentration. *Limnol. Oceanogr.* 42, 1–20. doi: 10.4319/lo.1997.42.1.0001
- Beisner, B. E., Haydon, D. T., and Cuddington, K. (2003). Alternative stable states in ecology. *Front. Ecol. Environ.* 1 (7), 376–382. doi: 10.1890/1540-9295(2003)001[0376:ASSIE]2.0.CO;2
- Bender, M. L., Orcharado, J., Dickson, M. L., Barber, R., and Lindley, S. (1999). *In vitro* O₂ fluxes compared with 14C production and other rate terms during the JGOFS Equatorial Pacific experiment. *Deep-Sea Res.* 46, 637–654. doi: 10.1016/S0967-0637(98)00080-6
- Bindoff, N. L., Cheung, W. W. L., Kairo, J. G., Aristegui, J., Guinder, V. A., Hallberg, R., et al. (2019). “Changing ocean, marine ecosystems, and dependent communities,” in *IPCC Special Report on the Ocean and Cryosphere in a Changing Climate*. Eds. H.-O. Pörtner, D. C. Roberts, V. Masson-Delmotte, P. Zhai, M. Tignor, E. Poloczanska, K. Mintenbeck, A. Alegria, M. Nicolai, A. Okem, J. Petzold, B. Rama and N. M. Weyer (Cambridge University Press, Cambridge, UK and New York, NY, USA), 447–587.
- Bittig, H. C., Körtzinger, A., Neill, C., van Ooijen, E., Plant, J. N., Hahn, J., et al. (2018). Oxygen optode sensors: principle, characterization, calibration, and application in the ocean. *Front. Mar. Sci.* 4. doi: 10.3389/fmars.2017.00429
- Bouman, H., Platt, T., Sathyendranath, S., and Stuart, V. (2005). Dependence of light-saturated photosynthesis on temperature and community structure. *Deep-Sea Res. I.* 52, 1284–1299. doi: 10.1016/j.dsr.2005.01.008
- Boyd, P. W., Claustre, H., Levy, M., Siegel, D. A., and Weber, T. (2019). Multi-faceted particle pumps drive carbon sequestration in the ocean. *Nature* 568, 327–335. doi: 10.1038/s41586-019-1098-2
- Brewer, P. G., and Riley, J. P. (1965). The automatic determination of nitrate in sea water. *Deep Sea Res. Oceanographic Abstracts* 12 (6), 765–772. doi: 10.1016/0011-7471(65)90797-7
- Carlson, C. A., del Giorgio, P. A., and Herndl, G. J. (2007). Microbes and the dissipation of energy and respiration: from cells to ecosystems. *Oceanography* 20 (2), 89–100. doi: 10.5670/oceanog.2007.52
- Carpenter, S. R., Arani, B. M. S., Van Nes, E. H., Scheffer, M., and Pace, M. L. (2022). Resilience of phytoplankton dynamics to trophic cascades and nutrient enrichment. *Limnol. Oceanogr.* 67, S258–S265. doi: 10.1002/lno.11913
- Cassar, N., Wright, S. W., Thomson, P. G., Trull, T. W., Westwood, K. J., de Salas, M., et al. (2015). The relation of mixed-layer net community production to phytoplankton community composition in the Southern Ocean. *Global Biogeochem. Cycles* 29, 446–462. doi: 10.1002/2014GB004936
- Claustre, H., Johnson, K. S., and Takeshita, Y. (2020). Observing the global ocean with biochemical-Argo. *Annu. Rev. Mar. Sci.* 12, 23–48. doi: 10.1146/annurev-marine-010419-010956
- del Giorgio, P. A., Cole, J. J., and Ciberis, A. (1997). Respiration rates in bacteria exceed phytoplankton production in unproductive aquatic systems. *Nature* 385, 148–151. doi: 10.1038/385148a0
- del Giorgio, P. A., and Williams, P. (2005). “The global significance of respiration in aquatic ecosystems: From single cells to the biosphere,” in *Respiration in Aquatic Ecosystems*. Eds. P. A. del Giorgio and P. Williams (New York: Oxford University Press, New York), 267–303.
- Duarte, C. M., and Agustí, S. (1998). The CO₂ balance of unproductive aquatic ecosystems. *Science* 281 (5374), 234–236. doi: 10.1126/science.281.5374.234
- Duarte, C. M., Regaudie-de-Gioux, A., Arrieta, J. M., Delgado-Huertas, A., and Agustí, S. (2013). The oligotrophic ocean is heterotrophic. *Ann. Rev. Mar. Sci.* 5, 551–569. doi: 10.1146/annurev-marine-121211-172337
- Ducklow, H. W., and Doney, S. C. (2013). What is the metabolic state of the oligotrophic ocean? *A. Debate. Ann. Rev. Mar. Sci.* 5, 525–533. doi: 10.1146/annurev-marine-121211-172331
- Falkowski, P. G. (1981). Light-shade adaptation and assimilation numbers. *J. Plankton Res.* 3 (2), 203–216. doi: 10.1093/plankt/3.2.203
- Falkowski, P. G., Barber, R. T., and Smetacek, V. (1998). Biogeochemical controls and feedbacks on ocean primary production. *Science* 281 (5374), 200–206. doi: 10.1126/science.281.5374.200
- Finkel, Z. V. (2007). “Does phytoplankton cell size matter? The evolution of modern marine food webs,” in *Evolution of Aquatic Photoautotrophs*. Eds. P. G. Falkowski and A. H. Knoll (Academic Press, San Diego), 333–350.
- Ford, D., Tilstone, G. H., Shutler, J. D., Kitidis, V., Lobanova, P., Schwarz, J., et al. (2021). Wind speed and mesoscale processes drive net autotrophy in the South Atlantic Ocean. *Remote Sens. Env.* 260, 112435. doi: 10.1016/j.rse.2021.112435
- Gasol, J. M., del Giorgio, P. A., and Duarte, C. M. (1997). Biomass distribution in marine planktonic communities. *Limnol. Oceanogr.* 42 (6), 1353–1363. doi: 10.4319/lo.1997.42.6.1353
- Grassoff, K., Erhardt, M., and Kremling, M. (1983). *Methods of seawater analysis*. 2nd edn (Verlag Chemie, Weinheim), 419.
- Grodsky, S. A., Carton, J. A., and McClain, C. R. (2008). Variability of upwelling and chlorophyll in the equatorial Atlantic. *Geophysical Res. Lett.* 35 (3), 1–6. doi: 10.1029/2007GL032466
- Gruber, N., Doney, S. C., Emerson, S. R., Gilbert, D., Kobayashi, T., Körtzinger, A., et al. (2010). “Adding oxygen to argo: developing a global *in situ* observatory for ocean deoxygenation and biogeochemistry,” in *Proceedings of OceanObs’09: Sustained Ocean Observations and Information for Society*, Venice, Italy, 21–25 September 2009, Vol. 2, 12 (ESA Publication WPP-306), Paris, France, European Space Agency. doi: 10.5270/OceanObs09.cwp.39
- Guidi, L., Stemann, L., Jackson, J. A., Ibanez, F., Claustre, H., Legendre, L., et al. (2009). Effects of phytoplankton community on production, size and export of large aggregates: A world-ocean analysis. *Limnol. Oceanogr.* 54 (6), 1951–1963. doi: 10.4319/lo.2009.54.6.1951
- Haskell, W. Z. II, Fassbender, A. J., Long, J. S., and Plant, J. N. (2020). Annual net community production of particulate and dissolved organic carbon from a decade of biogeochemical profiling float observations in the Northeast Pacific. *Global Biogeochem. Cycles* 34, e2020GB006599. doi: 10.1029/2020GB006599
- Hemming, M. P., Kaiser, J., Boutin, J., Merlivat, L., Heywood, K. J., Bakker, D. C. E., et al. (2022). Net community production in the northwestern Mediterranean Sea from glider and buoy measurements. *Ocean Sci.* 18, 1245–1262. doi: 10.5194/os-18-1245-2022
- Holling, C. S. (1973). Resilience and stability of ecological systems. *Annu. Rev. Ecol. Syst.* 4, 1–23. doi: 10.1146/annurev.es.04.110173.000245
- Hull, T., Greenwood, N., Kaiser, J., and Johnson, M. (2016). Uncertainty and sensitivity in optode-based shelf-sea net community production estimates. *Biogeosciences* 13, 943–959. doi: 10.5194/bg-13-943-2016
- Intergovernmental Oceanographic Commission (1994). Protocols for the joint global ocean flux study (JGOFS) core measurements. Paris, France, UNESCO-IOC, 170pp. (Intergovernmental oceanographic commission manuals and guides: 29). *JGOFS Rep.* 19. doi: 10.25607/OBP-1409
- Johnson, K. S., Plant, J. N., Coletti, L. J., Jannasch, H. W., Sakamoto, C. M., Riser, S. C., et al. (2017). Biogeochemical sensor performance in the SOCCOM profiling float array. *J. Geophys. Res. Oceans* 122, 6416–6436. doi: 10.1002/2017JC012838
- Juranek, L. W., White, A. E., Dugenne, M., Henderikx Freitas, F., Dutkiewicz, S., Ribaut, F., et al. (2020). The importance of the phytoplankton “middle class” to ocean net community production. *Global Biogeochem. Cycles* 34, e2020GB006702. doi: 10.1029/2020GB006702
- Karl, D. M., Bidigare, R. R., and Letelier, R. M. (2002). “Sustained and aperiodic variability in organic matter production and phototrophic microbial community structure in the North Pacific Subtropical Gyre,” in *Phytoplankton Productivity: Carbon Assimilation in Marine and Freshwater Ecosystems*. Eds. P. J. B. Williams, D. N. Thomas and S. Colin (New York: Reynolds Blackwell Publishing Ltd), 222–264.
- Karl, D. M., Laws, E. A., Morris, P., Williams, P., and Emerson, S. (2003). Metabolic balance of the open sea. *Nature* 426, 32. doi: 10.1038/426032a
- Kjørboe, T. (1993). Turbulence, phytoplankton cell size and the structure of pelagic food webs. *Adv. Mar. Biol.* 29, 1–72. doi: 10.1016/S0065-2881(08)60129-7
- Kulk, Platt, T., Dingle, J., Jackson, T., Jönsson, B. F., Bouman, H. A., et al. (2020). Primary production, an index of climate change in the ocean: satellite-based estimates over two decades. *Remote Sens.* 12, 826. doi: 10.3390/rs12050826
- Laws, E. A. (1991). Photosynthetic quotients, new production and net community production in the open ocean. *Deep-Sea Res. I.* 38 (1), 143–167. doi: 10.1016/0198-0149(91)90059-O
- Laws, E. A., DiTullio, G. R., and Redalje, D. G. (1987). High phytoplankton growth and production rates in the North Pacific subtropical gyre. *Limnol. Oceanogr.* 32 (4), 905–918. doi: 10.4319/lo.1987.32.4.0905
- Legendre, L., and Le Fevre, J. (1989). “Hydrodynamical singularities as controls of recycled versus export production in oceans,” in *Productivity of the Oceans: Present and Past*. Eds. W. H. Berger, V. S. Smetacek and G. Wefer (John Wiley & Sons), 49–63.
- Legendre, L., and Rassoulzadegan, F. (1996). Food-web mediated export of biogenic carbon in oceans: environmental control. *Mar. Ecol. Prog. Ser.* 145, 179–193. doi: 10.3354/meps145179
- Longhurst, A. (1998). *Ecological Geography of the Sea* (Academic Press).
- Longhurst, A., Sathyendranath, S., Platt, T., and Caverhill, C. (1995). An estimate of global primary production in the ocean from satellite radiometer data. *J. Plank. Res.* 17 (6), 1245–1271. doi: 10.1093/plankt/17.6.1245
- Lozano, J., Aranguren-Gassis, M., García-Martín, E. E., González, J., Herrera, J. L., Hidalgo-Robatto, B., et al. (2021). Seasonality of phytoplankton cell size and the relation between photosynthesis and respiration in the Ria de Vigo (NW Spain). *Mar. Ecol. Prog. Ser.* 664, 43–58. doi: 10.3354/meps13669
- Marra, J. (2009). Net and gross productivity: weighing in with 14C. *Aquat. Microb. Ecol.* 56, 123–131. doi: 10.3354/ame01306
- Marra, J. (2012). Comment on “Measuring primary production rates in the ocean: Enigmatic results between incubation and non-incubation methods at Station ALOHA. *Global Biogeochem. Cycles* 26 (2). doi: 10.1029/2011GB004087
- Marra, J., Trees, C. C., and O’Reilly, J. E. (2007). Phytoplankton pigment absorption: A strong predictor of primary productivity in the surface ocean. *Deep-Sea Res. I.* 54, 155–163. doi: 10.1016/j.dsr.2006.12.001

- Marra, J. F., Lance, V. P., Vaillancourt, R. D., and Hargreaves, B. R. (2014). Resolving the ocean's euphotic zone. *Deep-Sea Res. I* 83, 45–50. doi: 10.1016/j.dsr.2013.09.005
- Mignot, A., D'Ortenzio, F., Taillandier, V., Cossarini, G., and Salon, S. (2019). Quantifying observational errors in Biogeochemical-Argo oxygen, nitrate, and chlorophyll a concentrations. *Geophysical Res. Lett.* 46, 4330–4337. doi: 10.1016/S0924-7963(99)00054-8
- Morel, A., Antoine, D., Babin, M., and Dandonneau, Y. (1996). Measured and modeled primary production in the northeast Atlantic (EUMELI JGOFS program): the impact of natural variations in photosynthetic parameters on model predictive skill. *Deep-Sea Res. I* 43, 1273–1304. doi: 10.1016/0967-0637(96)00059-3
- Olesen, M., Lundsgaard, C., and Andrushaitis, A. (1999). Influence of nutrients and mixing on the primary production and community respiration in the Gulf of Riga. *J. Mar. Sys.* 23, 127–143. doi: 10.1016/S0924-7963(99)00054-8
- Oudot, C., Gerard, R., Morin, P., and Gningue, I. (1988). Precise shipboard determination of dissolved oxygen (Winkler procedure) for productivity studies with a commercial system. *Limnol. Oceanogr.* 33, 146–150. doi: 10.4319/lo.1988.33.1.0146
- Pasquier, B., Holzer, M., Chamberlain, M. A., Matear, R. J., Bindoff, N. L., and Primeau, F. W. (2023). Optimal parameters for the ocean's nutrient, carbon, and oxygen cycles compensate for circulation biases but replumb the biological pump. *Biogeosciences* 20, 2985–3009. doi: 10.5194/egusphere-2023-363
- Regaudie-de-Gioux, A., and Duarte, C. M. (2013). Global patterns in oceanic planktonic metabolism. *Limnol. Oceanography* 58 (3), 977–986. doi: 10.4319/lo.2013.58.3.0977
- Reynolds, S., Mahaffey, C., Roussenov, V., and Williams, R. G. (2014). Evidence for production and lateral transport of dissolved organic phosphorus in the eastern subtropical North Atlantic. *Global Biogeochem. Cycles* 28. doi: 10.1002/2013GB004801
- Robinson, A., Bouman, H. A., Tilstone, G. H., and Sathyendranath, S. (2018). Size class dependent relationships between temperature and phytoplankton photosynthesis-Irradiance parameters in the Atlantic Ocean. *Front. Mar. Sci.* 4. doi: 10.3389/fmars.2017.00435
- Robinson, C., and Williams, P. (2005). "Respiration and its measurement in surface marine waters," in *Respiration in Aquatic Ecosystems*. Eds. P. A. d. Giorgio and P. Williams (New York: Oxford University Press, New York), 147–180.
- Serret, P., Fernández, E., Anadón, R., and Varela, M. (2001). Trophic control of biogenic carbon export in Bransfield and Gerlache Straits, Antarctica. *J. Plank. Res.* 23 (12), 1345–1136. doi: 10.1093/plankt/23.12.1345
- Serret, P., Fernandez, E., Robinson, C., Woodward, E. M. S., and Perez, V. (2006). Local production does not control the balance between plankton photosynthesis and respiration in the open Atlantic Ocean. *Deep-Sea Res. II* 53 (14–16), 1611–1628. doi: 10.1016/j.dsr2.2006.05.017
- Serret, P., Robinson, C., Aranguren-Gassis, M., Garcia-Martin, E. E., Gist, N., Kitidis, V., et al. (2015). Both respiration and photosynthesis determine the scaling of plankton metabolism in the oligotrophic ocean. *Nat. Commun.* 6, 6961. doi: 10.1038/ncomms7961
- Serret, P., Robinson, C., Fernández, E., Teira, E., Tilstone, G., and Pérez, V. (2009). Predicting plankton net community production in the Atlantic Ocean. *Deep-Sea Res. Part II* 56, 941–953. doi: 10.1016/j.dsr2.2008.10.006
- Signorini, S. R., Franz, B. A., and McClain, C. R. (2015). Chlorophyll variability in the oligotrophic gyres: mechanisms, seasonality and trends. *Front. Mar. Sci.* 2. doi: 10.3389/fmars.2015.00001
- Smith, E. M., and Kemp, W. M. (2001). Size structure and the production/respiration balance in a coastal plankton community. *Limnol. Oceanogr.* 46 (3), 473–485. doi: 10.4319/lo.2001.46.3.0473
- Smyth, T. J., Tilstone, G. H., and Groom, S. B. (2005). Integration of radiative transfer into satellite models of ocean primary production. *J. Geophys. Res. Oceans* 110, C10014. doi: 10.1029/2004JC002784
- Soria-Piriz, S., García-Robledo, E., Papaspyrou, S., Aguilar, V., Seguro, I., Acuña, J., et al. (2017). Size fractionated phytoplankton biomass and net metabolism along a tropical estuarine gradient. *Limnol. Oceanogr.* 62, S309–S326. doi: 10.1002/lno.10562
- Tarran, G. A., Heywood, J. L., and Zubkov, M. V. (2006). Latitudinal changes in the standing stocks of eukaryotic nano- and picophytoplankton in the Atlantic Ocean. *Deep-Sea Res. II* 53 (14–16), 1516–1529. doi: 10.1016/j.dsr2.2006.05.004
- Tilstone, G. H., Smyth, T. J., Poulton, A., and Hutson, R. (2009). Measured and remotely sensed estimates of primary production in the Atlantic Ocean from 1998 to 2005. *Deep Sea-Res. II* 56 (15), 918–930. doi: 10.1016/j.dsr2.2008.10.034
- Tilstone, G. H., Xie, Y., Robinson, C., Serret, P., Raitsoo, D. E., Powell, T., et al. (2015). Satellite estimates of net community production indicate predominance of net autotrophy in the Atlantic Ocean. *Remote Sens. Environ.* 164, 254–269. doi: 10.1016/j.rse.2015.03.017
- Tremblay, J. E., and Legendre, L. (1994). A model for the size-fractionated biomass and production of marine phytoplankton. *Limnol. Oceanogr.* 39 (8), 2004–2014. doi: 10.4319/lo.1994.39.8.2004
- Vikström, K., Tengberg, A., and Wikner, J. (2019). Improved accuracy of optode-based oxygen consumption measurements by removal of system drift and nonlinear derivation. *Limnol. Oceanogr.: Methods* 17, 179–189. doi: 10.1002/lom3.10297
- Wang, S., Lin, Y., Gifford, S., Eveleth, R., and Cassar, N. (2018). Linking patterns of net community production and marine microbial community structure in the western North Atlantic. *ISME J.* 12, 2582–2595. doi: 10.1038/s41396-018-0163-4
- Welschmeyer, N. A. (1994). Fluorometric analysis of chlorophyll a in the presence of chlorophyll b and pheopigments. *Limnol. Oceanogr.* 39, 1985–1992. doi: 10.4319/lo.1994.39.8.1985
- Westberry, T. K., Silsbe, G. M., and Behrenfeld, M. J. (2023). Gross and net primary production in the global ocean: An ocean color remote sensing perspective. *Earth-Sci. Rev.* 237, 104322. doi: 10.1016/j.earscirev.2023.104322
- Westberry, T. B., Williams, P. J. B., and Behrenfeld, M. J. (2012). Global net community production and the putative net heterotrophy of the oligotrophic oceans. *Global Biogeochem. Cycles* 26, GB4019. doi: 10.1029/2011GB004094
- Wikner, J., Vikström, K., and Verma, A. (2023). Regulation of marine plankton respiration: A test of models. *Front. Mar. Sci.* 10. doi: 10.3389/fmars.2023.1134699
- Williams, P. J. B. (1998). The balance of plankton respiration and photosynthesis in the open oceans. *Nature* 394, 55–57. doi: 10.1038/27878
- Williams, P. J. B., Morris, P., and Karl, D. M. (2004). Net community production and metabolic balance at the oligotrophic ocean site, station ALOHA. *Deep-Sea Res. I* 51, 1563–1578. doi: 10.1016/j.dsr.2004.07.001
- Williams, P. B., Quay, P. D., Westberry, T. K., and Behrenfeld, M. J. (2013). The oligotrophic ocean is autotrophic. *Ann. Rev. Mar. Sci.* 5, 535–549. doi: 10.1146/annurev-marine-121211-172335
- Wilson, J. D., Andrews, O., Katavouta, A., de Melo Virissimo, F., Death, R. M., Adloff, M., et al. (2022). The biological carbon pump in CMIP6 models: 21st century trends and uncertainties. *PNAS* 119 (29), e2204369119. doi: 10.1073/pnas.2204369119
- Wu, J., Lee, Z., Xie, Y., Goes, J., Shang, S., Marra, J. F., et al. (2021). Reconciling between optical and biological determinants of the euphotic zone depth. *J. Geophysical Res.: Oceans* 126, e2020JC016874. doi: 10.1029/2020JC016874
- Zubkov, M., Seligh, M. A., Burkill, P. H., and Leakey, R. J. G. (2000). Picoplankton community structure on the Atlantic Meridional Transect: a comparison between seasons. *Prog. Oceanography* 45, 369–386. doi: 10.1016/S0079-6611(00)00008-2